

β ,*meso*-Acetylenyl-Bridged, Asymmetrical, Porphyrin Dyads – Synthesis, Spectral, Electrochemical and Computational Studies

Meesala Yedukondalu,^[a] Dilip K. Maity,^{*[b]} and Mangalampalli Ravikanth^{*[a]}

Keywords: Molecular devices / FRET / Density functional calculations / Porphyrin dyads / Heteroporphyrins / Acetylenyl bridge

The first examples of β ,*meso*-acetylenyl-bridged, asymmetrical, covalently linked, porphyrin dyads, containing two different subunits, such as ZnN₄P-N₃OP (**1**), ZnN₄P-N₃SP (**2**), ZnN₄P-N₂SOP (**4**) and ZnN₄P-N₂S₂P (**6**), were synthesized by the coupling of a β -acetylenyl, ZnN₄ porphyrin with a *meso*-bromoheteroporphyrin under mild, Pd⁰-catalyzed, coupling conditions. The dyads containing different types of metal-free subunits, such as N₄P-N₃SP (**3**), N₄P-N₂SOP (**5**) and N₄P-N₂S₂P (**7**), were synthesized by the demetallation of the corresponding dyads. The seven β ,*meso*-acetylenyl dyads **1–7** were characterized by NMR, MS, absorption, fluorescence and electrochemical techniques. The NMR, absorption and electrochemical studies support an electronic interaction be-

tween the subunits in all seven dyads. The steady-state fluorescence studies on dyads **1–7** support an efficient energy transfer from the donor (ZnN₄ or N₄) subunit to the acceptor heteroporphyrin subunit upon excitation of the ZnN₄/N₄ subunit. First-principle-based, quantum-chemical studies carried out on dyads **1**, **2**, **4** and **6** further support an electronic interaction between the donor and acceptor subunits. The computational studies also predict significant tuning of the electronic energy levels in these dyads with the modification of the porphyrin core of the acceptor groups. The calculations support the experimental results of efficient donor→acceptor energy transfer in these dyads.

Introduction

Asymmetrical porphyrin dyads containing different macrocycles such as porphyrin–phthalocyanine,^[1] porphyrin–chlorin,^[2] porphyrin–corrole^[3] and porphyrin–heteroporphyrin^[4] have receiving attention recently, because the singlet-state energy levels of two macrocycles in these types of dyads are arranged favorably for efficient transfer of energy in the metal-free state. Earlier reports on covalently linked porphyrin dyads were mainly limited to systems containing two of the same type of macrocycles such as two normal porphyrins (N₄ core). The energy gradient between two of the same macrocycles was created by selectively metallating one of the porphyrin units and keeping the other macrocycle in the metal-free form. Thus, covalently linked porphyrin dyads^[5] connected by various types of linkers, containing a metalloporphyrin (e.g. as a Zn^{II} or Mg^{II} derivative) as an energy donor and a metal-free porphyrin as an energy acceptor, have been synthesized. These compounds demonstrated an efficient energy transfer in the sin-

glet state from the metalloporphyrin subunit to the metal-free subunit. However, the absorption bands of the donor metalloporphyrin often have good overlap with the absorption bands of the acceptor porphyrin. Hence, it is often difficult to selectively excite the donor subunit. Furthermore, the emission bands of the donor and acceptor subunits also overlap to a great extent, which prevents the estimation of the amount of donor emission quenched. These problems can be circumvented by using two different types of macrocycles whose absorption and emission bands do not overlap significantly. Lindsey and co-workers^[6] and others synthesized porphyrin–phthalocyanine dyads and higher oligomers, in which the phthalocyanine subunit absorbs at lower energy and acts as an energy acceptor, and the porphyrin subunit absorbs at higher energy and acts as an energy donor. In porphyrin–phthalocyanine dyads, there is a good separation between absorption and emission bands; hence, the selective excitation of the donor subunit and the estimation of energy-transfer parameters are possible in these systems. Recently, we and others synthesized several covalent, *meso*-diarylethyne-bridged, asymmetrical dyads^[7] containing porphyrin (N₄ core) and heteroporphyrin subunits (N₃X and N₂X₂ cores; X = O and S) and showed the possibility of efficient energy transfer in the singlet state from the porphyrin to the heteroporphyrin subunit. A perusal of the literature reveals that such asymmetrical dyads are rare, and more such systems are needed to explore their potential for various applications. It is established that the electronic in-

[a] Department of Chemistry, Indian Institute of Technology, Mumbai 400076, India
Fax: +91-22-25767152
E-mail: ravikanth@chem.iitb.ac.in

[b] Theoretical Chemistry Section, Chemistry Group, Bhabha Atomic Research Centre, Mumbai 400085, India
E-mail: dkmaity@barc.gov.in

Supporting information for this article is available on the WWW under <http://dx.doi.org/10.1002/ejoc.200901362>.

interactions between the two subunits in dyads can be modulated by connecting two porphyrins in different orientations such as *meso,meso*, β ,*meso* and β,β , which facilitates electronic delocalization within the dyads.^[8] Tuning the energy gaps between the highest doubly occupied molecular orbitals (HOMOs) and the lowest unoccupied molecular orbitals (LUMOs) of such extended π -conjugated systems should play a vital role in optimizing the performance of electronic devices based on these active organic components. However, there are very few reports available on dyads in which the β -position of the first porphyrin is connected to the *meso*-position of second porphyrin. Therien et al.,^[9] Osuka et al.^[10] and others^[11] have synthesized β ,*meso*-linked dyads connected either directly or by ethyne and phenyl bridges. However, these dyads are symmetrical in nature, containing two of the same type of subunits (N_4 core).

In this paper, we report four new, asymmetrical, β ,*meso*-acetylenyl-bridged dyads containing porphyrin and heteroporphyrin subunits such as ZnN_4P-N_3OP (**1**), ZnN_4P-N_3SP (**2**), ZnN_4P-N_2SOP (**4**) and $ZnN_4P-N_2S_2P$ (**6**) and three metal-free dyads such as N_4P-N_3SP (**3**), N_4P-N_2SOP (**5**) and $N_4P-N_2S_2P$ (**7**), as shown in Figure 1. The dyads **1**, **2**, **4** and **6** were prepared from readily available porphyrin building blocks under Pd^0 -catalyzed coupling conditions, and dyads **3**, **5** and **7** were prepared by the demetallation of the corresponding dyads. Preliminary photophysical studies supported an efficient energy transfer from the ZnN_4/N_4 subunit to the heteroporphyrin subunit upon the selective excitation of the ZnN_4/N_4 subunit. The structure and electronic properties of dyads **1**, **2**, **4** and **6**, along with their appropriate porphyrin monomers, were calculated by applying density-functional-based electronic-structure theory with all the electron, Gaussian, atomic, basis functions. Appropriate MO contour plots were generated and visualized

to determine any definite orbital interaction present between the donor and acceptor moieties of the dyads through the linker. Frontier orbital diagrams were also generated, and the effect of the β ,*meso* connection in the porphyrin dyads on the HOMO–LUMO gap were correlated to the observed differences in the experimental results. The visualization of appropriate MOs suggests an interaction between the donor and acceptor moieties of the dyads through the linker.

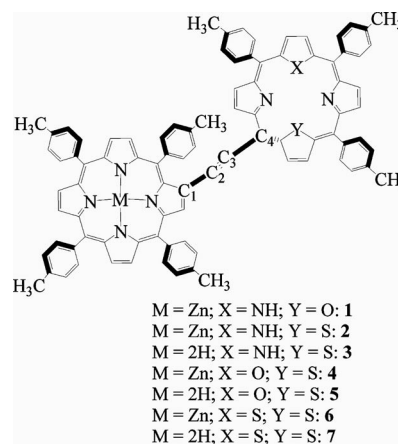


Figure 1. β ,*meso*-acetylenyl-bridged, asymmetrical dyads **1–7**.

Results and Discussion

The required monofunctionalized porphyrin and heteroporphyrin building blocks **8–15**, for the synthesis of β ,*meso*-acetylenyl-bridged dyads **1–7**, are shown in Figure 2. The β -bromoporphyrin building block [2-bromo-5,10,15,20-tet-

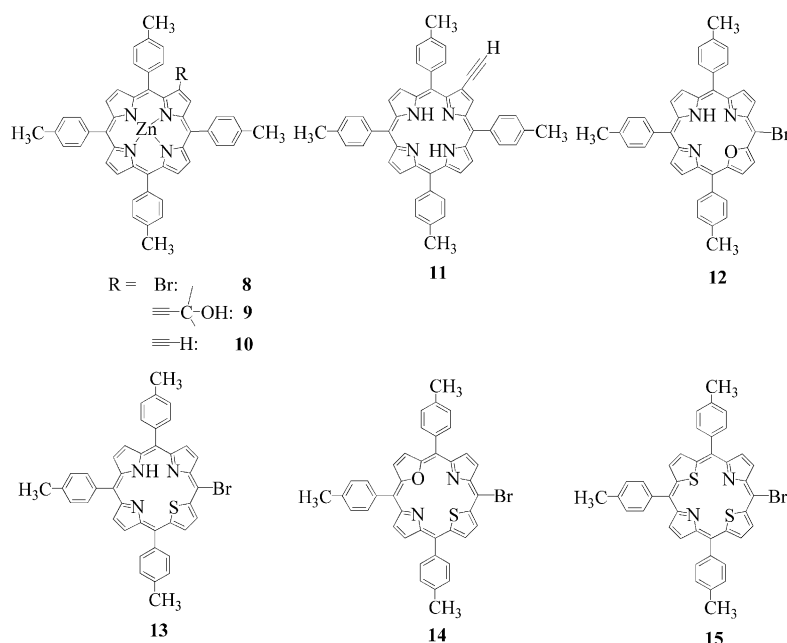
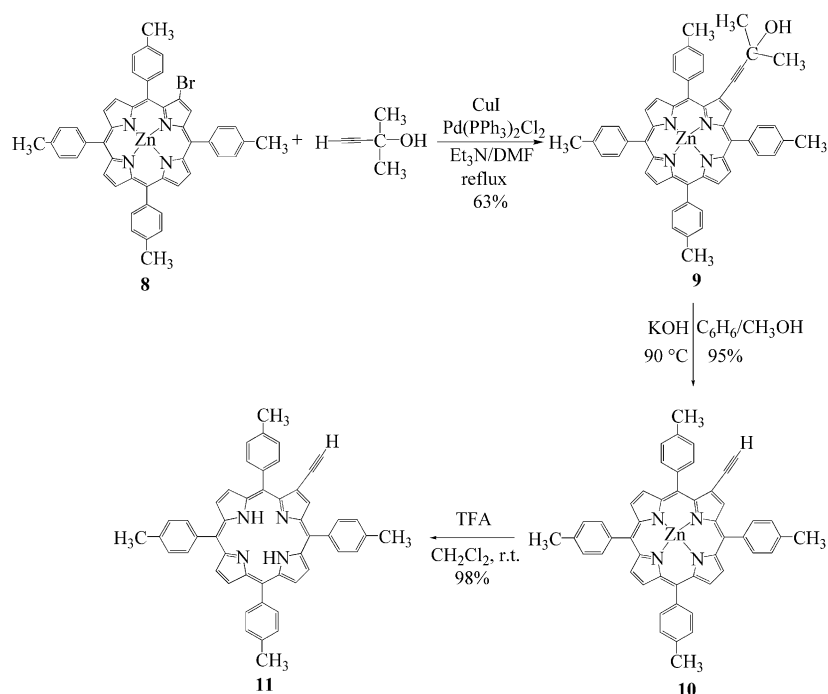


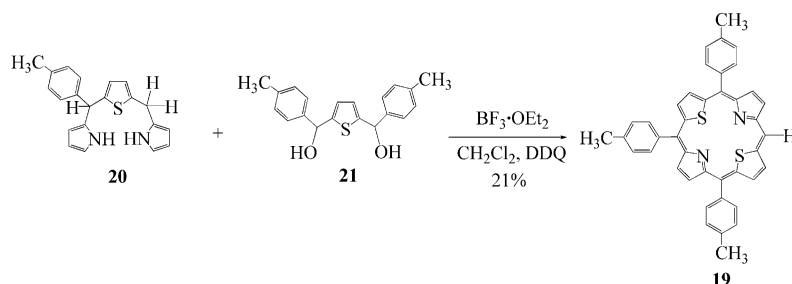
Figure 2. Functionalized monomers **8–15**.

ra(*p*-tolyl)porphyrinato]zinc(II) (**8**) was synthesized according to a literature procedure.^[12] The *meso*-bromoporphyrin building blocks such as 5-bromo-10,15,20-tri(*p*-tolyl)-21-oxaporphyrin (**12**) and 5-bromo-10,15,20-tri(*p*-tolyl)-21-thiaporphyrin (**13**) were synthesized from monomeric, *meso*-unsubstituted porphyrins such as 10,15,20-tri(*p*-tolyl)-21-oxaporphyrin (**16**) and 10,15,20-tri(*p*-tolyl)-21-thiaporphyrin (**17**), respectively, according to our previously reported procedure.^[13] The building block [2-ethynyl-5,10,15,20-tetra(*p*-tolyl)porphyrinato]zinc(II) (**10**) was prepared by an alternate route, starting from [2-{(3-methyl-3-hydroxybut-1-yn-1-yl)}-5,10,15,20-tetra(*p*-tolyl)porphyrinato]zinc(II) (**9**, Scheme 1). Compound **9** was prepared by treating **8** with 2-methyl-3-butyn-2-ol in the presence of a catalytic amount of CuI/Pd(PPh₃)₂Cl₂ in Et₃N/DMF at reflux for 16 h, followed by silica gel column chromatographic purification. Compound **9** was confirmed by the molecular ion peak in the ESI mass spectrum and elemental analysis, which matched the expected composition. In the ¹H NMR spectrum of **9**, the seven β-pyrrole signals appeared as four sets of signals at δ = 8.70–9.20 ppm, consistent with the asym-

metric nature of the compound. In the absorption spectrum of **9**, one strong Soret band at 431 nm and two Q-bands at 559 and 597 nm were observed, which were slightly red-shifted compared to **8**. Compound **10** was prepared by deprotecting **9** with KOH in C₆H₆/CH₃OH at 90 °C overnight, followed by column chromatographic purification on silica gel. Compound **10** was confirmed by a singlet at δ = 3.27 ppm, corresponding to the CCH proton in the ¹H NMR spectrum and a molecular ion peak in the ESI mass spectrum. Compound **11** was prepared by treating **10** with TFA in CH₂Cl₂, followed by column chromatographic purification. The molecular ion peak in the ESI mass spectrum and a signal at δ = –2.58 ppm corresponding to the two inner NH protons in the ¹H NMR spectrum confirmed the identity of **11**. Porphyrins 5-bromo-10,15,20-tri(*p*-tolyl)-21-oxa-23-thiaporphyrin (**14**) and 5-bromo-10,15,20-tri(*p*-tolyl)-21,23-dithiaporphyrin (**15**) were prepared from monomeric, *meso*-unsubstituted porphyrins 10,15,20-tri(*p*-tolyl)-21-oxa-23-thiaporphyrin (**18**)^[13] and 10,15,20-tri(*p*-tolyl)-21,23-dithiaporphyrin (**19**), respectively. Compound **18** was prepared as reported earlier,^[13] and porphyrin **19**



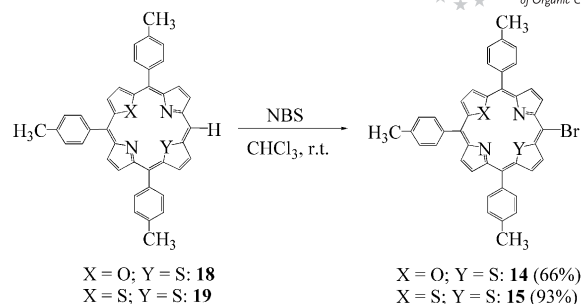
Scheme 1. Synthesis of 2-ethynyl-5,10,15,20-tetra(*p*-tolyl)porphyrin (**11**).



Scheme 2. Synthesis of *meso*-free dithiaporphyrin **19**.

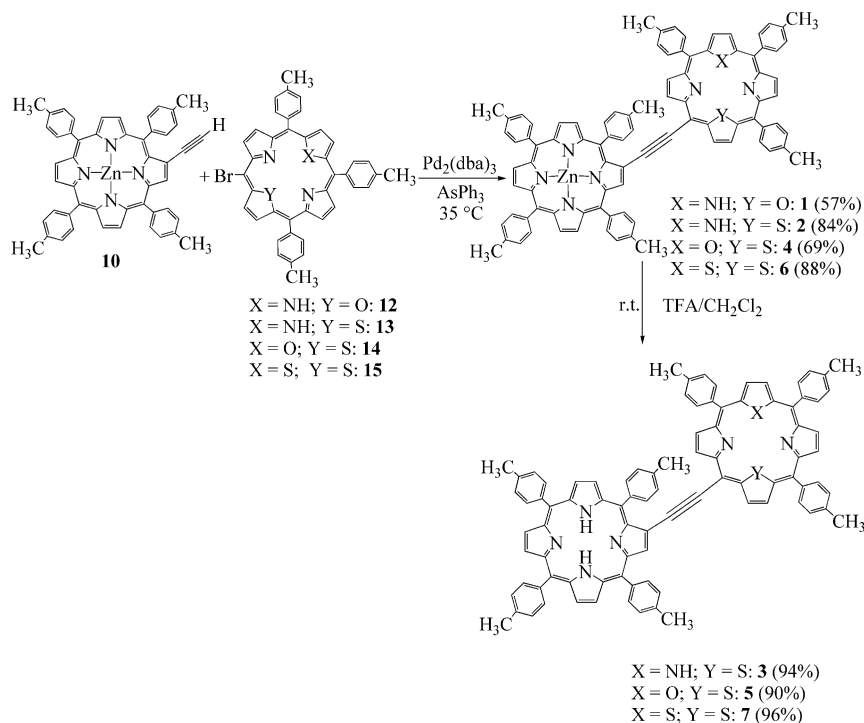
was prepared by adopting an alternate methodology, as shown in Scheme 2. The condensation of 1 equiv. of asymmetrical 5-(*p*-tolyl)-10,15,17-trihydro-16-thiatripyrrane (**20**) with 1 equiv. of symmetrical 2,5-[hydroxy(*p*-tolyl)methyl]thiophene (**21**) in CH_2Cl_2 under mild acidic conditions,^[14] followed by purification on silica gel, yielded **19** as single product in decent yield. The advantage of this methodology over our previously reported method^[13] is that no scrambling was noted in this reaction, and the desired compound was obtained as a single product in higher yield. Porphyrins **14** and **15** were prepared by treating 1 equiv. of porphyrins **18** and **19**, respectively, with 1 equiv. of *N*-bromosuccinimide (NBS) in CHCl_3 at room temperature (Scheme 3). The molecular ion peak in the ESI mass spectrum confirmed the identity of **14** and **15**. In the ^1H NMR spectrum, the *meso*-proton, the signal of which generally appears at $\delta \approx 10.6$ – 10.8 ppm in **18** and **19**, was absent in **14** and **15**. The absorption spectra of **14** and **15** showed four Q-bands and one Soret band, which were bathochromically shifted relative to those of porphyrins **18** and **19**, respectively, due to the presence of bromine at the *meso* position.

Covalently linked, asymmetrical, β -*meso*-acetylenyl-bridged dyads **1**, **2**, **4** and **6**, containing two different subunits, were prepared by coupling β -ethynyl Zn^{II} porphyrin **10** with *meso*-bromoporphyrins **12**, **13**, **14** and **15**, respectively, in the presence of $\text{Pd}_2(\text{dba})_3/\text{AsPh}_3$ in $\text{C}_6\text{H}_6/\text{Et}_3\text{N}$ at 35°C for 4 h.^[15] The reaction progress was monitored by TLC analysis, and the reaction was stopped after the complete disappearance of the starting monomers and the appearance of a new spot, corresponding to the desired dyad. The crude, asymmetrical dyads were purified by silica gel column chromatography and afforded dyads **1**, **2**, **4** and **6**



Scheme 3. Synthesis of 5-bromo-10,15,20-tri(*p*-tolyl)-21-oxa-23-thiaporphyrin (**14**) and 5-bromo-10,15,20-tri(*p*-tolyl)-21,23-dithiaporphyrin (**15**).

in 55–85% yield (Scheme 4). The coupling reactions worked smoothly and required one simple chromatographic purification to afford dyads in decent yields. Dyads **1**, **2**, **4** and **6** were freely soluble in common organic solvents and characterized by various spectroscopic and electrochemical techniques. The molecular ion peaks in the MALDI-TOF mass spectrum confirmed the identity of dyads **1**, **2**, **4** and **6**. Dyads **1**, **2**, **4** and **6**, along with their corresponding monomers **10**, **12**, **13**, **14** and **15**, respectively, were characterized in detail by NMR spectroscopy, and the data of selected protons are presented in Table 1. The ^1H NMR spectra of dyads **1**, **2**, **4** and **6** were very clean, and the resonances of the dyads were assigned on the basis of the ^1H NMR spectra observed for the corresponding monomers and ^1H - ^1H COSY and NOESY spectra recorded for the dyads. A representative spectrum of dyad **2**, along with the spectra of the corresponding monomers **10** and **13**, over a selected re-



Scheme 4. Synthesis of asymmetrical, porphyrin dyads **1**–**7**.

gion, is shown in Figure 3a, and the ^1H - ^1H COSY spectrum of dyad **2** is shown in Figure 3b. A close inspection of Figure 3 and the data presented in Table 1 indicates that only the signals of selected protons such as the β -pyrrole protons, represented as H_a , H_b , H_c and the β -thiophene/ β -furan protons experienced downfield shifts due to the porphyrin current effect. In general, it is apparent that there are more signals for the dyads than there are for the monomers, supporting the asymmetric nature of the dyads. In all four dyads (**1**, **2**, **4** and **6**), the signal of the β -pyrrole proton of the ZnN_4 subunit, which is adjacent to the ethyne linker (H_a), experienced a ca. 0.5 ppm downfield shift relative to the same signal in the ZnN_4 monomer **10**, indicating the alteration of the ring current of the ZnN_4 subunit in the dyads. The signals of the β -thiophene/ β -furan and other β -pyrrole protons of the heteroporphyrin subunits experienced slight alterations in their chemical shifts. Furthermore, the signal of the inner NH proton of the N_3S subunit in dyad **2** experienced a downfield shift of ca. 0.5 ppm, and the inner NH signal of the N_3O subunit in dyad **1** was not

observed, due to the more basic nature of the N_3O subunit. In addition to the observations described above, we also note that the *meso*-(*p*-tolyl) group of the ZnN_4 subunit, which is adjacent to the acetylenic bridge, experienced the ring current of the heteroporphyrin subunit. The signal of the *meso*-(*p*-tolyl) group, which is perpendicular to the ZnN_4 subunit but coplanar with the heteroporphyrin subunit, exhibited evidence of interaction with a ring current by its upfield shift, clearly observed for the *meta*-protons, represented as H_d , in the ^1H NMR spectra. Furthermore, the signals of the methyl protons of the *meso*-(*p*-tolyl) group, represented as H_g , also experienced a ca. 1.2 ppm upfield shift, clearly seen in the NOESY spectrum (see the Supporting Information). This kind of upfield shift of the central *meso*-(*p*-tolyl) groups had previously been observed for similar dimeric porphyrin systems.^[16] These observations were further supported by ab initio, quantum-chemical calculations. Thus, the NMR study supported an interaction between the two subunits in all four β ,*meso*-acetylenyl-bridged, asymmetrical dyads **1**, **2**, **4** and **6**.

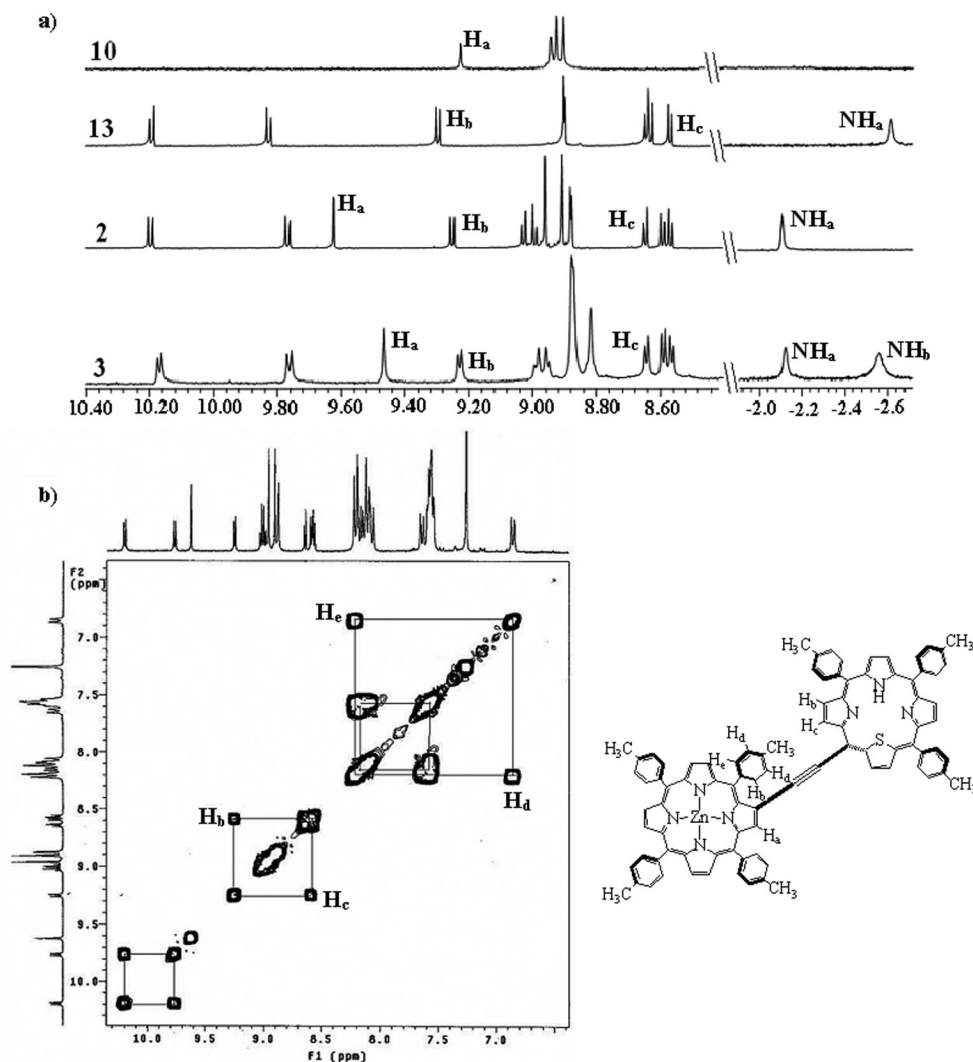


Figure 3. NMR spectra of dyads and their corresponding monomers. (a) Comparison of partial ^1H NMR spectra of dyads **2** and **3** with monomers **10** and **13**, recorded in CDCl_3 . (b) ^1H - ^1H COSY spectrum of dyad **2**.

Table 1. ^1H NMR chemical shifts (δ in ppm) of selected protons of dyads **1–7**, along with their corresponding monomers, recorded in CDCl_3 .

Entry	Compound	β -Thiophene/ β -furan	β -Pyrrole			Inner NH
			H_a	H_b	H_c	
1	10	–	9.13 (s)	–	–	–
2	11	–	9.15 (s)	–	–	–2.58 (s)
3	12	10.04 (d), 9.49 (d)	–	9.29 (d)	8.57 (d)	–
4	13	10.18 (d), 9.82 (d)	–	9.30 (d)	8.57 (d)	–2.62 (s)
5	14	10.15 (d), 9.66 (d) (β -thio), 9.65 (d), 9.37 (d) (β -fur)	–	9.35 (d)	8.64 (d)	–
6	15	10.20 (d), 9.76 (d), 9.64 (s)	–	9.31 (d)	8.70 (d)	–
7	1	10.45 (d), 9.76 (d)	9.62 (s)	9.03 (d)	8.66 (d)	–
8	2	10.20 (d), 9.76 (d)	9.62 (s)	9.24 (d)	8.65 (d)	–2.10 (s) (N_3SP)
9	3	10.16 (d), 9.75 (d)	9.46 (s)	9.22 (d)	8.63 (d)	–2.12 (s) (N_3SP), –2.56 (s) (N_4P)
10	4	9.96 (d), 9.64 (d) (β -thio), 9.63 (d), 9.33 (d) (β -fur)	9.63 (s)	9.22 (d)	8.60 (d)	–
11	5	9.92 (d), 9.63 (d) (β -thio), 9.63 (d), 9.30 (d) (β -fur)	9.48 (s)	9.20 (d)	8.60 (d)	–2.56 (s) (N_4)
12	6	10.20 (d), 9.70 (d), 9.63 (d)	9.62 (s)	9.28 (d)	8.67 (d)	–
13	7	10.17 (d), 9.70 (d), 9.63 (d)	9.47 (s)	9.25 (d)	8.66 (d)	–2.56 (s) (N_4)

The metal-free dyads $\text{N}_4\text{P-N}_3\text{SP}$ (**3**), $\text{N}_4\text{P-N}_2\text{SOP}$ (**5**) and $\text{N}_4\text{P-N}_2\text{S}_2\text{P}$ (**7**) were synthesized by the demetallation of dyads **2**, **4** and **6**, respectively. The demetallation was carried out by treating the corresponding metallated dyad in CH_2Cl_2 with TFA for 15 min. The progress of the reaction was monitored by TLC analysis and absorption spectroscopy. After the standard workup, the crude, metal-free dyads were purified on a short silica gel column and afforded pure dyads **3**, **5** and **7**, in ca. 90% yield. The molecular ion peak in the mass spectra and the broad signal for the two inner NH protons of the N_4 subunit at $\delta \approx -2.56$ ppm in the ^1H NMR spectra confirmed the identity of the dyads. Dyads **3**, **5** and **7** showed similar ^1H NMR spectral features and exhibited slight shifts for the signals of selected protons, as observed for metallated dyads **1**, **2**, **4** and **6** (Table 1).

Absorption Properties of Dyads 1–7

The absorption spectra of dyads **1–7** and their corresponding monomers in CH_2Cl_2 were recorded at room temperature, and the results are listed in Table 2. A comparison of the absorption spectra of dyads **2** and **3**, along with monomers **10** and **13**, is shown in Figure 4. As is clear from Figure 4 and Table 2, the dyads exhibit split Soret bands and bathochromic shifts of both the Q- and Soret bands relative to their corresponding monomers. For example, dyad **2**, containing ZnN_4 and N_3S subunits, showed four Q-bands at 528, 570, 600 and 699 nm and two Soret bands at 428 and 450 nm. In this dyad, the bands at 450, 528 and 699 nm were exclusively due to the N_3S subunit; the band at 428 nm was exclusively due to the ZnN_4 subunit, and the bands at 570 and 600 nm were due to both the ZnN_4 and

Table 2. Absorption data of dyads **1–7**, along with their corresponding monomers, recorded in CH_2Cl_2 .

Entry	Compound	Soret bands		Q-bands			
		λ [nm] ($\log \epsilon$)					
1	10	428 (5.75)	–	558 (4.18)	597 (3.67)	–	–
2	11	426 (5.72)	521 (4.35)	557 (4.03)	598 (3.87)	655 (3.88)	–
3	12	430 (5.18)	516 (4.05)	551 (3.45)	620 (3.11)	–	681 (3.23)
4	13	422 (5.35)	512 (4.16)	577 (3.67)	610	–	677
5	14	434 (5.73)	517 (4.02)	547 (3.47)	–	649 (3.14)	717 (3.32)
6	15	438 (5.48)	516 (4.29)	549 (3.79)	638 (3.12)	–	702 (3.61)
7	1	431 (5.60), 456 (5.35)	484 (4.32)	561 (4.63)	608 (4.60)	–	680 (3.75)
8	2	428 (5.64), 450 (5.73)	528 (4.42)	570 (4.81)	600 (4.41)	–	699 (4.13)
9	3	426 (5.18), 449 (5.29)	524 (4.24)	571 (4.25)	600 (4.01)	655 (3.60)	699 (3.72)
10	4	429 (5.35), 450 (5.27)	526 (4.32)	565 (4.49)	596 (4.05)	–	733 (4.02)
11	5	425 (5.08), 454 (5.19)	525 (4.16)	571 (4.19)	601 (3.92)	657 (3.51)	721 (3.69)
12	6	427 (5.72), 455 (5.77)	530 (4.55)	570 (4.86)	595 (4.60)	–	721 (4.28)
13	7	428 (5.45), 453 (5.31)	525 (4.58)	567 (4.57)	600 (4.36)	657 (3.95)	734 (4.17)

N_3S subunits. All these absorption bands of dyad **2** were redshifted relative to those of the corresponding ZnN_4 and N_3S monomers (Table 2). Similarly, the metal-free dyad **3**, containing N_4 and N_3S subunits, showed five Q-bands at 524, 571, 600, 655 and 699 nm and two Soret bands at 426 and 449 nm, which were redshifted relative to those of corresponding monomers. Furthermore, we note that in dyads 1–7, the absorption bands corresponding to the heteroporphyrin subunit exhibited more redshifts than did the ZnN_4/N_4 unit.

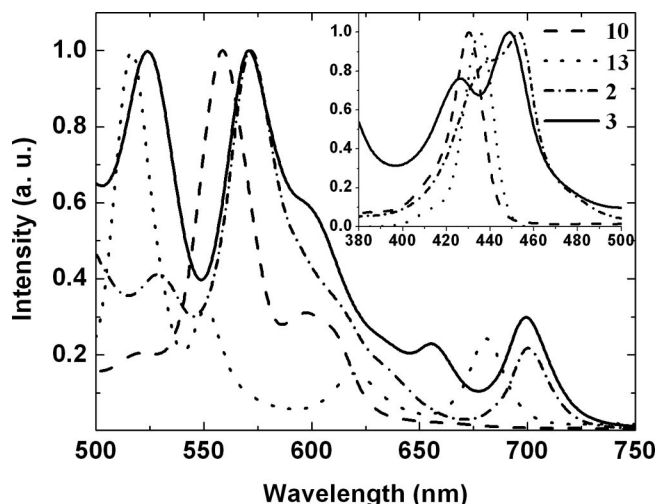


Figure 4. Normalized Q-bands and Soret band (inset) absorption spectra of dyads **2** and **3** along with their monomers **10** and **13**, recorded in CH_2Cl_2 .

Electrochemical Properties of Dyads 1–7

The electrochemical properties of dyads 1–7 were studied by cyclic voltammetry (CV) and differential pulse voltammetry at a scan rate of 50 mV/s using tetrabutylammonium perchlorate as the supporting electrolyte (0.1 M) in CH_2Cl_2 . The oxidation and reduction waves of dyads **2** and **6** are shown in Figure 5, and the redox data along with the data of **2**, **6** and their corresponding monomers are presented in Table 3. In general, the dyads exhibited two or three oxidations and two to four reductions. The oxidations and reductions are reversible or quasi-reversible ($\Delta E_p = 60$ –120 mV) and, in some cases, irreversible. The redox waves of the dyads were assigned by comparison with the redox potentials of the corresponding porphyrin monomers. For example, dyad **2**, containing ZnN_4 and N_3S subunits, exhibited four reductions at -1.03 , -1.37 , -1.55 and -1.68 V. The first two reduction waves at -1.03 and -1.37 V were assigned to the first and second reductions of the N_3S subunit on the basis of the fact that the N_3S porphyrin is easier to reduce than the $Zn^{II}N_4$ porphyrin.^[17] The reductions at -1.55 and -1.68 V were assigned to the first and second reductions of the ZnN_4 subunit. Similarly, dyad **2** showed three oxidations at 0.80, 1.11 and 1.52 V. The first oxidation at 0.80 V was assigned to the ZnN_4 subunit since the ZnN_4 porphyrin is easier to oxidize than the N_3S porphyrin. The oxidation at 1.52 V was exclusively assigned to the oxidation of the N_3S subunit, and the oxidation at 1.11 V was due to the oxidation of both the ZnN_4 and N_3S subunits. However, in dyads **3**, **5** and **7**, containing the metal-free N_4 subunit and heteroporphyrin subunit, the oxidations overlapped, but the reductions could be assigned to the subunits

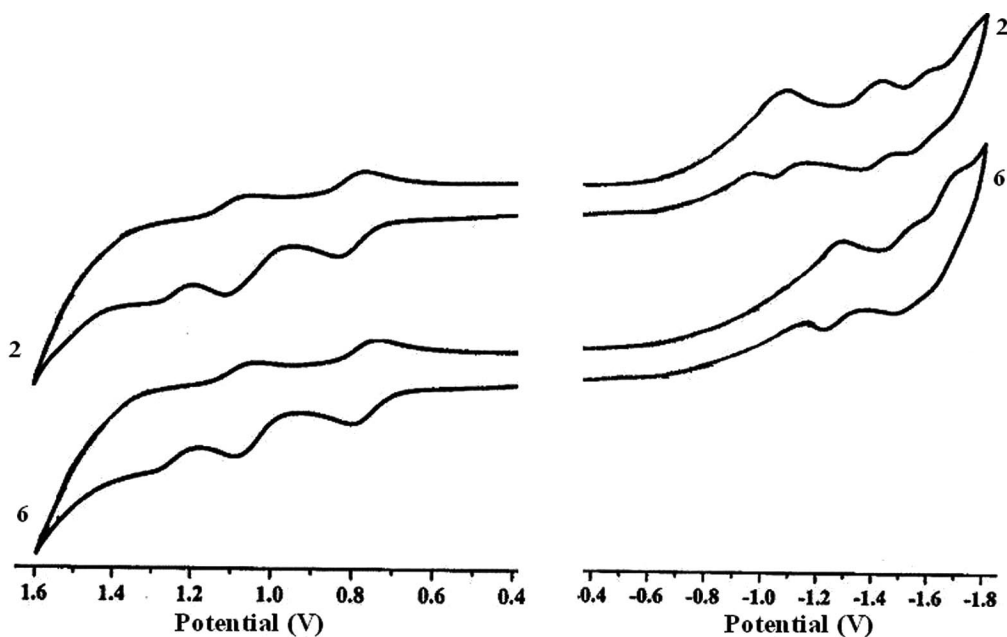


Figure 5. Oxidation and reduction waves of dyads **2** and **6** in CH_2Cl_2 containing 0.1 M TBAP as the supporting electrolyte, recorded at a 50 mV s⁻¹ scan speed.

Table 3. Electrochemical redox data [V] of dyads **2–7** and their corresponding monomers recorded in CH₂Cl₂ containing 0.1 M TBAP as the supporting electrolyte at a scan rate of 50 mV/s. $E_{1/2}$ values are reported relative to SCE.

Entry	Compound	Oxidation					Reduction			E_{CT} [M ⁺ , M ⁻]	E_{0-0} [eV]
		$E_{1/2}$ [V] vs. SCE (ΔE_P [mV])					$E_{1/2}$ [V] vs. SCE (ΔE_P [mV])				
1	10	0.78 (88)	1.08 (88)	–	–	–	–	–1.48 (97)	–1.65 (108)	–	2.03
2	11	–	1.01	1.41	–	–1.12 (58)	–	–1.40 (89)	–	–	1.90
3	13	–	1.15	–	1.53 (88)	–0.96 (67)	–1.39 (79)	–	–	–	1.80
4	14	–	–	–	–	–1.18	–	–1.50	–	–	1.72
5	15	–	1.19	–	1.58 (86)	–1.14 (78)	–1.25 (95)	–	–	–	1.75
6	2	0.80 (70)	1.11 (73)	–	1.52	–1.03 (52)	–1.37 (94)	–1.55 (74)	–1.68 (57)	1.83	–
7	3	–	1.10	1.42	–	–1.00 (56), –1.11 (79)	–	–1.40 (94)	–	2.10	–
8	4	0.80 (70)	1.10 (80)	–	–	–1.17	–	–1.49 (54)	–1.63 (57)	1.97	–
9	5	–	1.09	1.40	–	–1.11 (57)	–	–1.42 (74), –1.48 (131)	–	2.20	–
10	6	0.80 (68)	1.11 (77)	–	1.55	–	–1.22 (81)	–1.50	–1.62 (73)	2.02	–
11	7	–	1.01, 1.16	1.43	–	–1.10 (74)	–1.32	–1.44 (66)	–	2.11	–

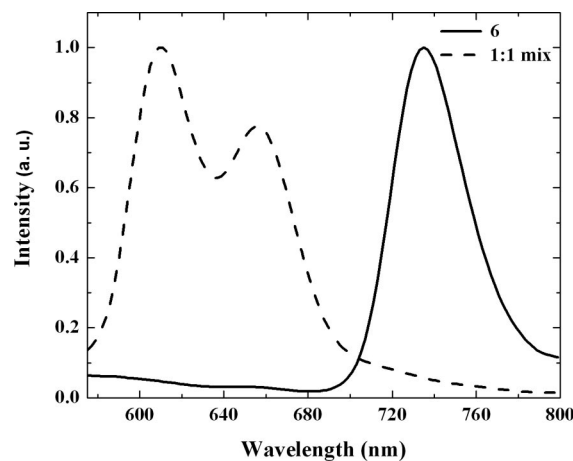
by comparison with the corresponding monomer data. A close inspection of the redox data of the dyads indicated that the subunit in the dyads exhibited slightly altered oxidations and reductions compared to their corresponding monomers, supporting an interaction between the subunits in dyads **1–7**.

Excited-State Properties of Dyads **1–7**

The steady-state fluorescence properties of dyads **1–7** were studied in CH₂Cl₂, and the data are presented in Table 4. The metallated dyads **1**, **2**, **4** and **6** were excited at 550 nm, where the ZnN₄ subunit absorbs strongly, or 530 nm, where the heteroporphyrin subunit absorbs strongly. A comparison of the fluorescence spectra of **6** with that of a 1:1 mixture of the corresponding monomers **10** and **15**, excited at 550 nm, is shown in Figure 6. Upon excitation of dyads **1**, **2**, **4** and **6** at 550 nm, one would expect a strong emission from the ZnN₄ subunit, as was observed for a 1:1 mixture of **10** and **15** (Figure 6). A careful inspection of Figure 6 and the data in Table 4 indicates that the emission from the ZnN₄ subunit was quenched by ca. 99%, and the strong emission observed originated from heteroporphyrin subunit. However, when dyads **1**, **2**, **4** and **6** were excited at 530 nm, where the heteroporphyrin subunit absorbs strongly, the emission originated from the heteroporphyrin subunit. Furthermore, the excitation spectra recorded for all four dyads, using an emission wavelength of 730 nm, closely matched those of their respective absorption spectra. These observations strongly support an efficient energy transfer from the ZnN₄ subunit to the heteroporphyrin subunit in dyads **1**, **2**, **4** and **6**. Similarly, the fluorescence properties of metal-free dyads **3**, **5** and **7** were studied by using excitation wavelengths of 420 and 450 nm. The fluorescence spectra of dyads **3**, **5** and **7**, recorded at 420 nm, are shown in Figure 7, and the relevant data is presented in Table 4. When dyads **3**, **5** and **7** were excited at 450 nm, where the heteroporphyrin subunit absorbs strongly, the emission originated exclusively from the

Table 4. Emission data of dyads **1–7**, recorded in CH₂Cl₂.

Entry	Compound	λ_{ex} [nm]	Porphyrin subunit	Φ_f	% quenched
1	H ₂ TPP ^[a]	420	–	0.11	–
2	ZnTPP ^[a]	550	–	0.033	–
3	OTPPH ^[a]	420	–	0.037	–
4	STPPH ^[a]	430	–	0.016	–
5	SOTPP ^[a]	430	–	0.005	–
6	S ₂ TPP ^[a]	435	–	0.007	–
7	1	550	ZnN ₄ em	0.0001	97.2
8	1	530	N ₃ Oem	0.0035	–
9	2	550	ZnN ₄ em	0.0006	98.2
10	2	530	N ₃ Sem	0.014	–
11	4	550	ZnN ₄ em	0.0002	99.4
12	4	530	N ₂ SOem	0.0048	–
13	6	550	ZnN ₄ em	0.0002	99.4
14	6	530	N ₂ S ₂ em	0.0068	–
15	3	420	N ₄ em	0.0015	98.7
16	3	450	N ₃ Sem	0.015	–
17	5	420	N ₄ em	0.0003	98.7
18	5	450	N ₂ SOem	0.005	–
19	7	420	N ₄ em	0.0011	99
20	7	450	N ₂ S ₂ em	0.0057	–

[a] Taken from ref.^[17]Figure 6. Comparison of emission spectra of dyad **6** and a 1:1 mixture of monomers **10/15**, recorded at λ_{ex} = 550 nm in CH₂Cl₂.

heteroporphyrin subunit, as expected. However, when dyads **3**, **5** and **7** were excited at 420 nm, where the metal-free N_4 subunit absorbs strongly, the emission from the N_4 subunit was quenched by 98%, and the strong emission originated mainly from the heteroporphyrin subunit, supporting an efficient energy transfer from the N_4 subunit to the heteroporphyrin subunit. Thus, the steady-state fluorescence studies clearly support an efficient energy transfer from the ZnN_4/N_4 subunit to the heteroporphyrin subunit in dyads **1–7**. Even though the energy transfer in the singlet state is the major process responsible for quenching the fluorescence of the donor ZnN_4/N_4 subunits in dyads **1–7**, a photoinduced electron transfer (PET) cannot be completely ruled out in these dyads. Hence, we evaluated the relationships of the energy levels for dyads **2** and **3** with Equations (1) and (2), respectively, using fluorescence and redox potential data.^[18]

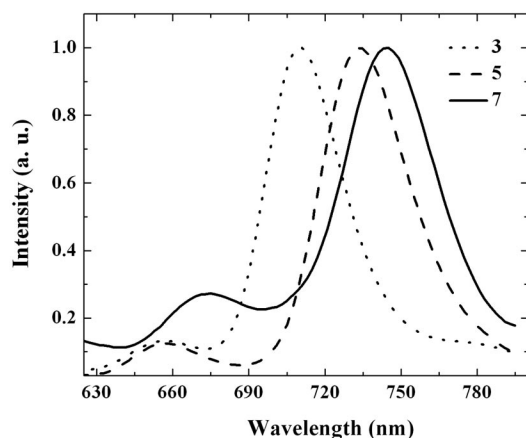


Figure 7. Normalized emission spectra of dyads **3**, **5** and **7**, recorded at $\lambda_{\text{ex}} = 420$ nm in CH_2Cl_2 .

$$\Delta G(^1ZnN_4P \rightarrow N_3S) = E_{\text{CT}}(ZnN_4P^+N_3S^-) - E_{0-0}(ZnN_4P) \quad (1)$$

$$\Delta G(^1N_4P \rightarrow N_3S) = E_{\text{CT}}(N_4P^+N_3S^-) - E_{0-0}(N_4P) \quad (2)$$

The singlet, excited and charge-transfer states for dyads **2** and **3** are shown in Figure 8. In dyad **2**, the charge-transfer state is lower than the singlet state of the donor ZnN_4 , whereas in dyad **3**, the charge-transfer state is higher than the singlet state of the donor N_4 porphyrin. Thus, the free energy change ΔG_{PET} is negative for dyad **2**, indicating that electron transfer is also possible in addition to energy transfer. However, in the case of dyad **3**, the ΔG_{PET} is positive, indicating that the PET is not possible, and energy transfer is the predominant process. More studies are required to probe the excited-state dynamics of these covalently linked dyads.

Quantum-Chemical Studies

To support the inferences drawn from the experimental results and to provide more insight into the electronic properties of these porphyrin-based dyads, quantum-chemical calculations were carried out by applying density functional theory. Equilibrium structures, calculated at the B3LYP/6-31G(d) level of theory for the four dyads **1**, **2**, **4** and **6**, are displayed with selected geometrical parameters for clarity in Figure 9. We note that the dihedral angle between the two subunits is ca. 70° , and the distance between the two subunits is ca. 4.05 \AA in all four dyads. Furthermore, the heteroporphyrin subunit in all four dyads deviates from planarity, as is evident from the calculated, fully optimized structures. The calculated distance between two opposite Ns in the heteroporphyrin subunit is quite different in these four dyads (Figure 9), showing a significant modification of

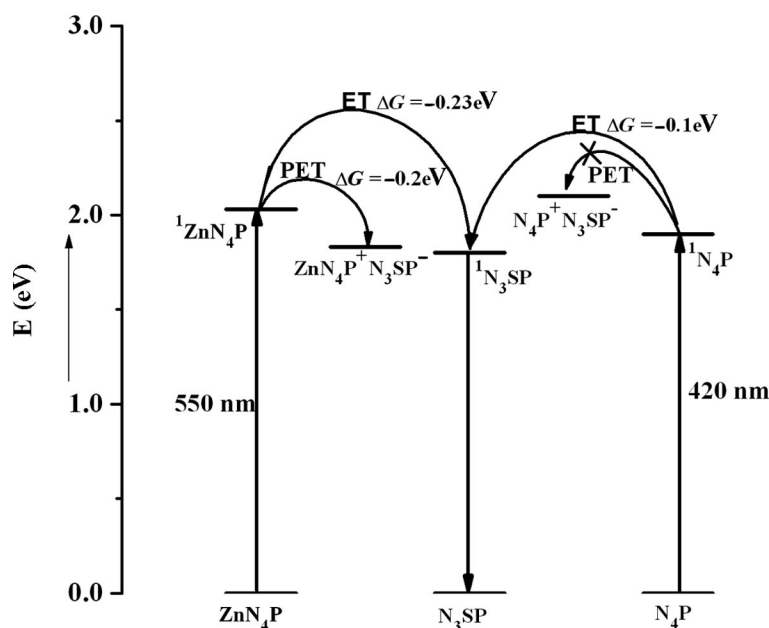


Figure 8. Energies of singlet and charge-transfer states of dyads **2** and **3**.

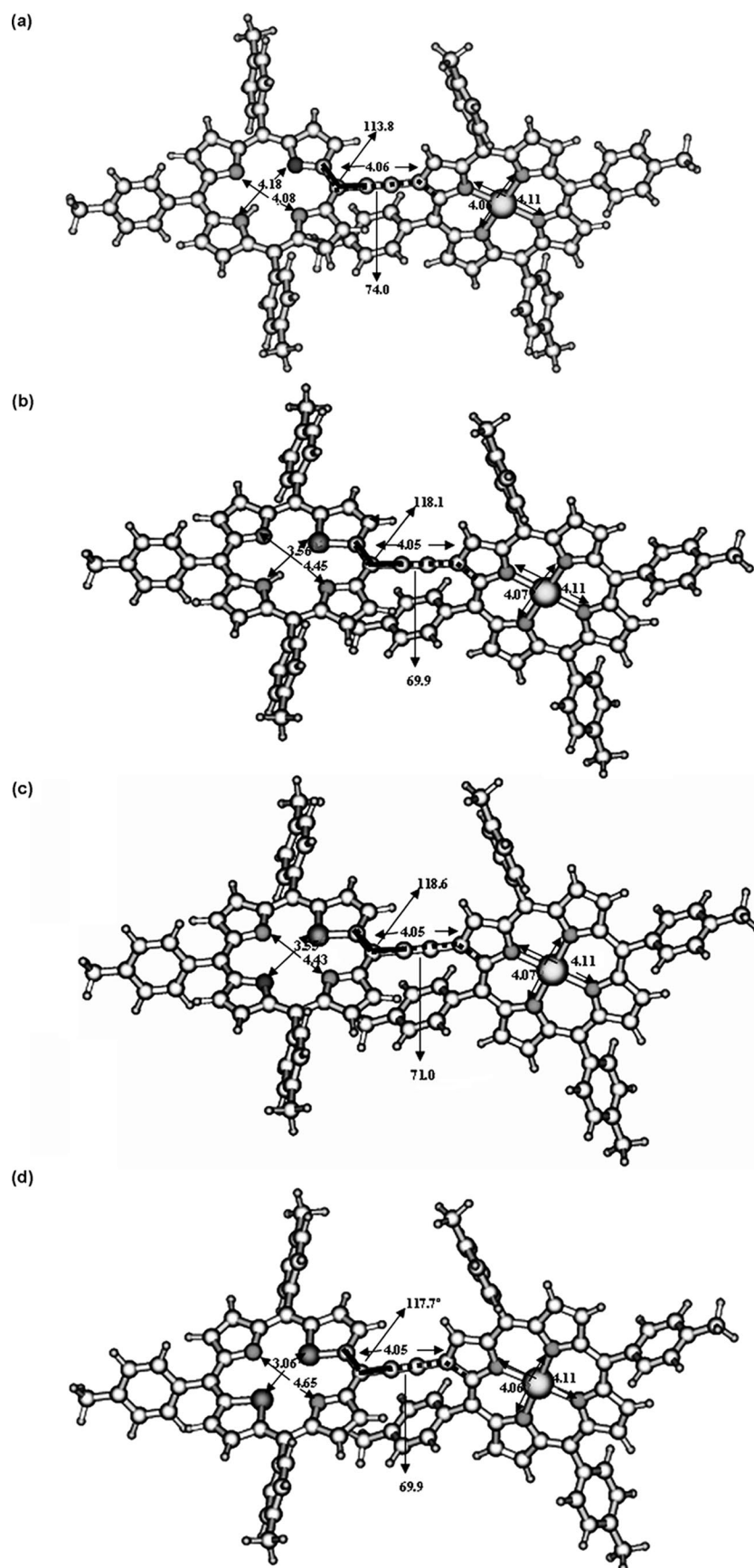


Figure 9. Calculated, optimized structures with selected geometrical parameters of dyads (a) 1, (b) 2, (c) 4 and (d) 6 at the B3LYP/6-31G(d) level of theory. Distances in Å; angles in °.

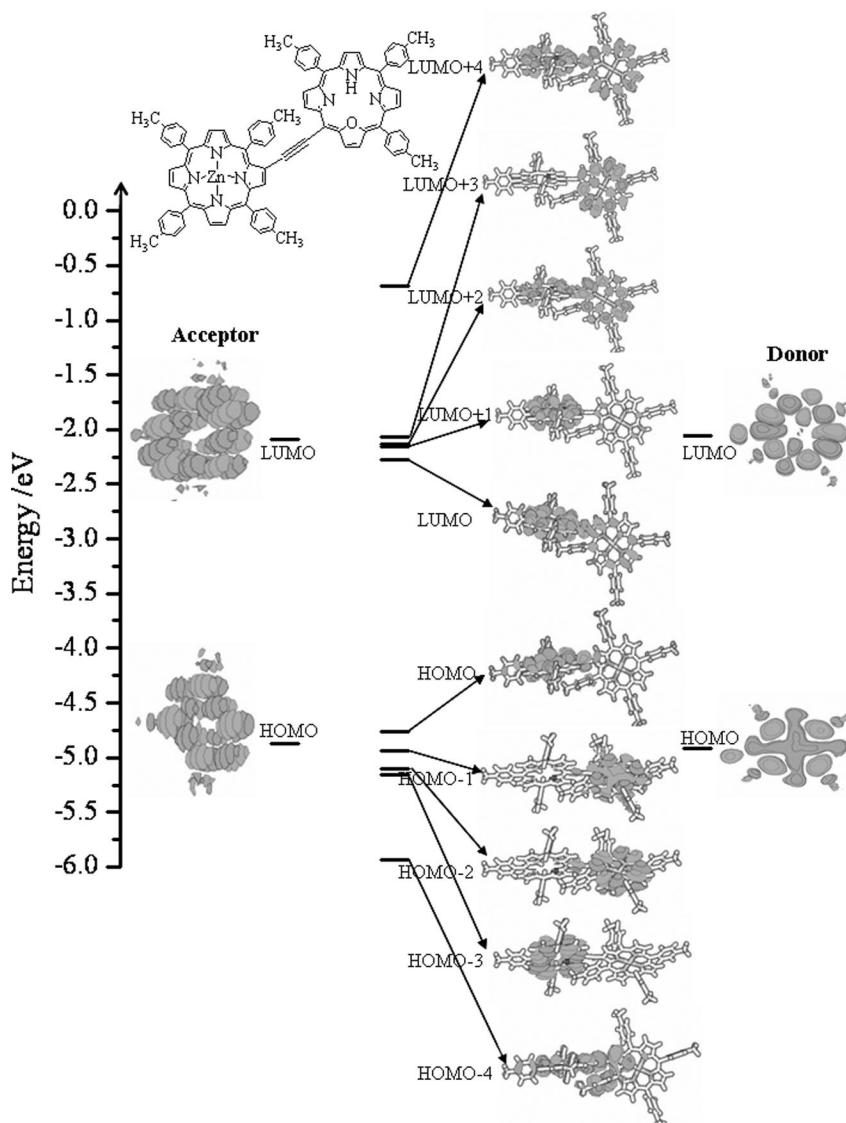


Figure 10. Frontier orbital correlation diagram for β ,*meso*, $\text{ZnN}_4\text{P-N}_3\text{OP}$, asymmetrical dyad **1**.

the core (acceptor). All the final, optimized, geometrical parameters of these dyads and their subunits are supplied in the Supporting Information in the form of Cartesian coordinates. Frontier orbitals (FO) were also calculated for dyads **1**, **2**, **4** and **6** and displayed in Figures 10, 11, 12 and 13, respectively, in the form of orbital correlation diagrams; the FOs and energies of the respective subunits are also shown. The present calculations also indicate that in all four dyads, the *meso*-phenyl group of the ZnN_4 subunit (donor) adjacent to the acetylenic bridge is parallel to the heteroporphyrin subunit (acceptor). This allows the *meso*-phenyl group of the donor to participate in π - π interactions with the acceptor subunit. This is clearly reflected in the ^1H - ^1H COSY spectra, which showed a doublet at $\delta = 6.9$ ppm for the two *ortho*-phenyl protons of the donor subunit in all the dyads (Figure 3b).

The HOMO in the FO correlation diagram of dyad **1** (Figure 10) indicates an extended π overlap between the N_3O acceptor and the C_1 atom of the ZnN_4 donor unit

through the acetylenic bridge. The LUMO manifests more extensive electronic delocalization between the two macrocycles. Higher-energy states like LUMO + 2 and LUMO + 4 exhibit a comprehensive π -electron delocalization between the donor ZnN_4 and acceptor N_3O subunits. Stable states like HOMO - 4 show extended π -electron delocalization within the dyad, from the acceptor N_3O subunit to the donor ZnN_4 subunit and extending to the *meso*-phenyl group of the ZnN_4 subunit, which is parallel to the acceptor N_3O subunit. The HOMO of dyad **1** is destabilized by 0.10 and 0.15 eV relative to those of the acceptor and donor, respectively, whereas the LUMO is stabilized by 0.10 and 0.13 eV with respect to those of the acceptor N_3O and donor ZnN_4 subunits, respectively (Figure 14a). These opposite energetic trends of the MOs reduces the HOMO-LUMO gap substantially to 2.58 eV for **1**, down from 2.86 and 2.78 eV for **10** and **16**, respectively. Table 5 provides the calculated HOMO-LUMO gaps for the dyads and their corresponding monomer subunits.

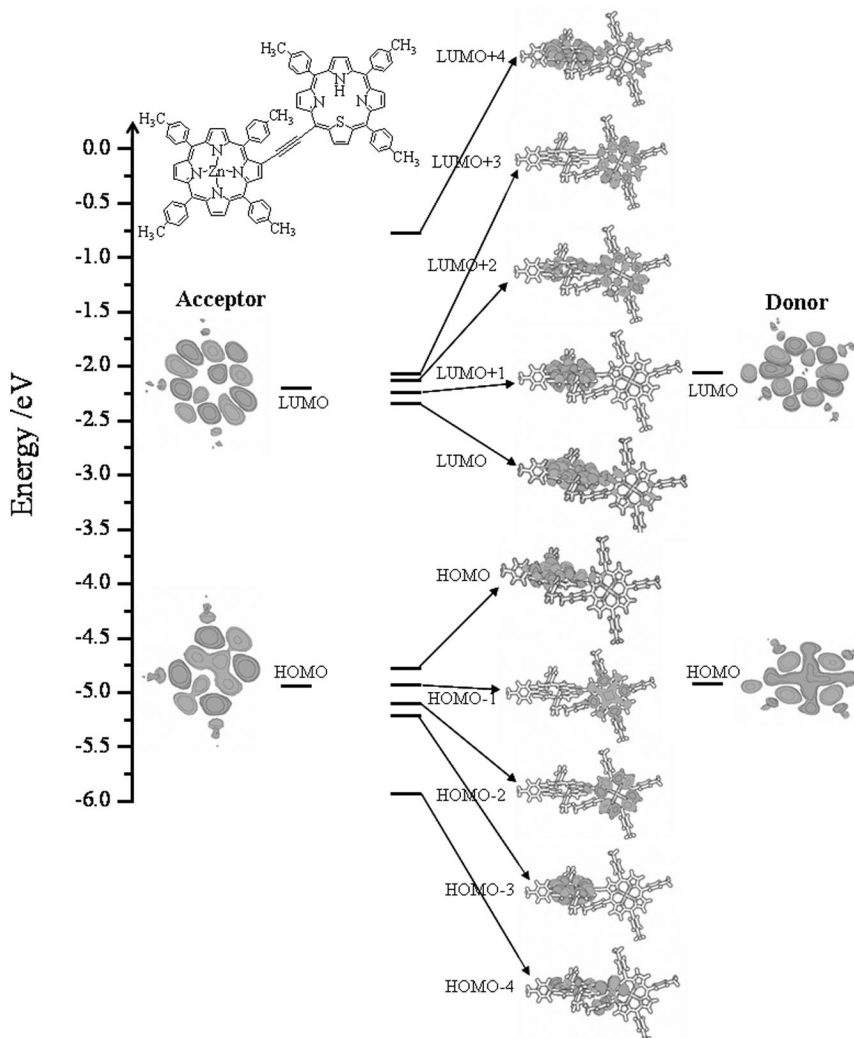


Figure 11. Frontier orbital correlation diagram for β ,*meso*, $\text{ZnN}_4\text{P-N}_3\text{SP}$, asymmetrical dyad **2**.

Similar results were obtained for dyad **2** in terms of the extended, π -electron delocalization from the acceptor N_3S to the donor ZnN_4 subunit in the case of HOMO - 4, LUMO + 2 and LUMO + 4, as depicted in Figure 11. However, the calculated HOMO–LUMO energy gap is 2.43 eV, which is lower than that of dyad **1**. The HOMO of dyad **2** is destabilized by 0.16 and 0.14 eV relative to those of the acceptor and donor, respectively, whereas the LUMO is stabilized by 0.16 and 0.29 eV with respect to those of the acceptor N_3S and donor ZnN_4 subunits, respectively. Figure 12 displays the FO correlation diagram of dyad **4**, showing selected MOs of the dyad and its constituent monomers. The visualization of the displayed MOs suggests significant electronic interactions between the acceptor N_2SO and the donor ZnN_4 subunits in the HOMO and LUMO states, as in dyads **1** and **2**. The HOMO of dyad **4** is destabilized by 0.17 and 0.14 eV relative to those of the acceptor and donor, respectively, whereas the LUMO is stabilized by 0.12 and 0.33 eV with respect to those of the acceptor N_2SO and donor ZnN_4 subunits, respectively. As a result, the calculated HOMO–LUMO energy gap is 2.38 eV for dyad **6**. Se-

lected MOs and energy levels of dyad **6** and its monomer constituents are displayed in Figure 13, which shows extended, π -electron delocalization between two subunits. The HOMO of dyad **6** is destabilized by 0.21 and 0.10 eV relative to those of the acceptor and donor, respectively, whereas the LUMO is stabilized by 0.13 and 0.38 eV with respect to those of the acceptor N_2S_2 and donor ZnN_4 subunits, respectively. Figure 14 depicts a comparative chart of HOMO–LUMO energy gaps in these four dyads and the corresponding monomer donor and acceptor subunits. It demonstrates that the modified core alters the HOMO–LUMO energy gap significantly, indicating electronic interactions in these newly synthesized, β ,*meso* dyads. Dyad **6** has the largest gap between HOMO energy levels of the donor and the acceptor (Figure 14), indicating that **6** experiences the largest energy transfer of these four dyads. The HOMO orbitals of these four dyads show that, apart from the linker, only atoms from the acceptors participate in this MO. However, atoms from both the donor and acceptor subunits participate in LUMO orbitals, showing that these systems are potential candidates for a molecular switch.

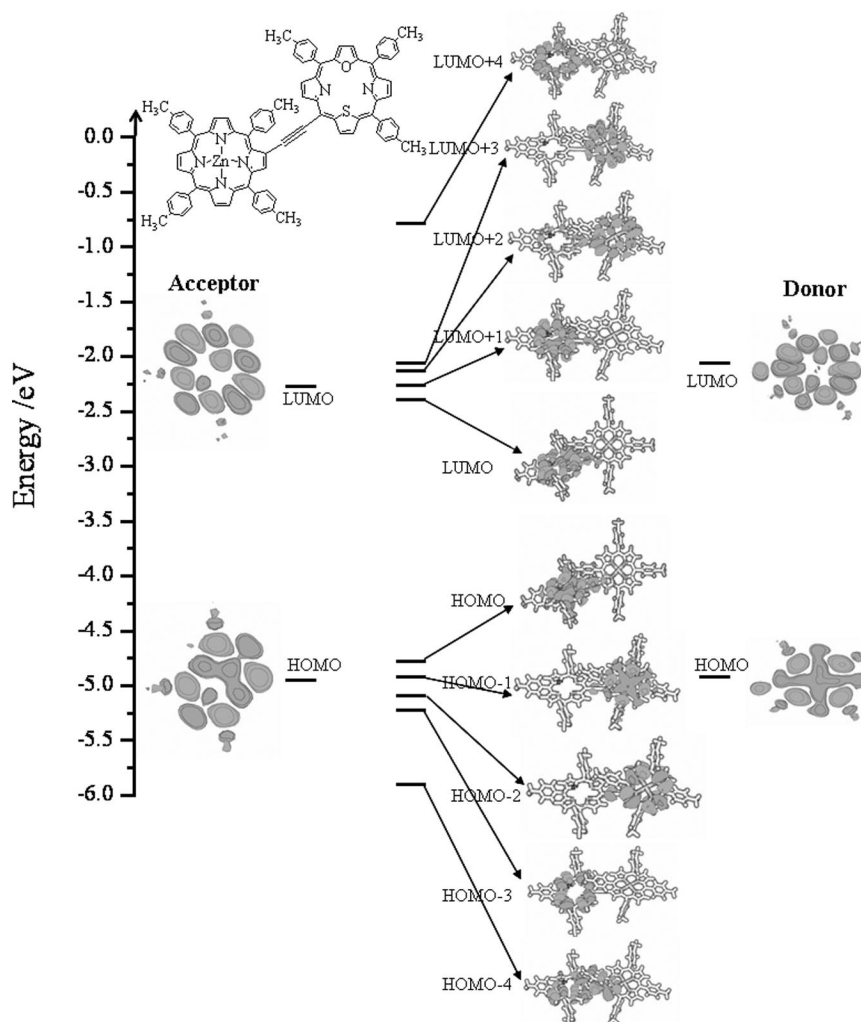


Figure 12. Frontier orbital correlation diagram for β ,*meso*, $\text{ZnN}_4\text{P-N}_2\text{SOP}$, asymmetrical dyad **4**.

Dyad **6** has the smallest HOMO–LUMO energy gap, and therefore, is the best candidate for molecular-level device applications among the β ,*meso*-substituted dyads reported herein.

Conclusions

We synthesized the first examples of covalently linked, β ,*meso*-acetylenyl-bridged, asymmetrical dyads containing a ZnN_4 subunit and a heteroporphyrin subunit such as N_3O , N_3S , N_2SO and N_2S_2 by the coupling of β -ethynyl ZnN_4 with a *meso*-bromoheteroporphyrin under mild, Pd^0 -catalyzed, coupling conditions. The coupling works well, and dyads containing two different subunits such as $\text{ZnN}_4\text{P-N}_3\text{OP}$ (**1**), $\text{ZnN}_4\text{P-N}_3\text{SP}$ (**2**), $\text{ZnN}_4\text{P-N}_2\text{SOP}$ (**4**) and $\text{ZnN}_4\text{P-N}_2\text{S}_2\text{P}$ (**6**) were obtained in decent yields. The dyads containing two metal-free subunits such as $\text{N}_4\text{P-N}_3\text{SP}$ (**3**), $\text{N}_4\text{P-N}_2\text{SOP}$ (**5**) and $\text{N}_4\text{P-N}_2\text{S}_2\text{P}$ (**7**) were obtained by demetallating the corresponding dyads with mild acid. The NMR, optical and electrochemical studies support an interaction between the two subunits. The steady-state fluorescence studies indicate an efficient energy transfer from the

ZnN_4/N_4 subunit to the heteroporphyrin subunit upon excitation of the ZnN_4/N_4 subunit. The computational studies carried out on asymmetrical dyads containing metalloporphyrin and heteroporphyrin subunits also support an interaction between the subunits. Our computational studies indicated that β ,*meso*-acetylenyl-bridged, asymmetrical, $\text{ZnN}_4\text{P-N}_2\text{S}_2\text{P}$ dyad **6** is the best potential candidate for molecular-level applications among the dyads presented herein. Currently, efforts are underway to explore these dyads in more detail using ultra-fast, photophysical studies.

Experimental Section

General: ^1H NMR spectra were recorded with a Varian 400 MHz instrument using tetramethylsilane (TMS) as an internal standard. ^{13}C NMR spectra were recorded with a Varian spectrometer operating at 100.6 MHz. All NMR experiments were carried out at room temperature in CDCl_3 with TMS as an internal standard. Absorption spectra were obtained with a Perkin–Elmer Lambda-35 instrument, and steady-state fluorescence spectra were obtained with a PC1 photon counting spectrofluorimeter, manufactured by ISS, USA. IR spectra were recorded with a Nicolet Impact-400 FTIR spectrometer, and ESI mass spectra were recorded with a Q-

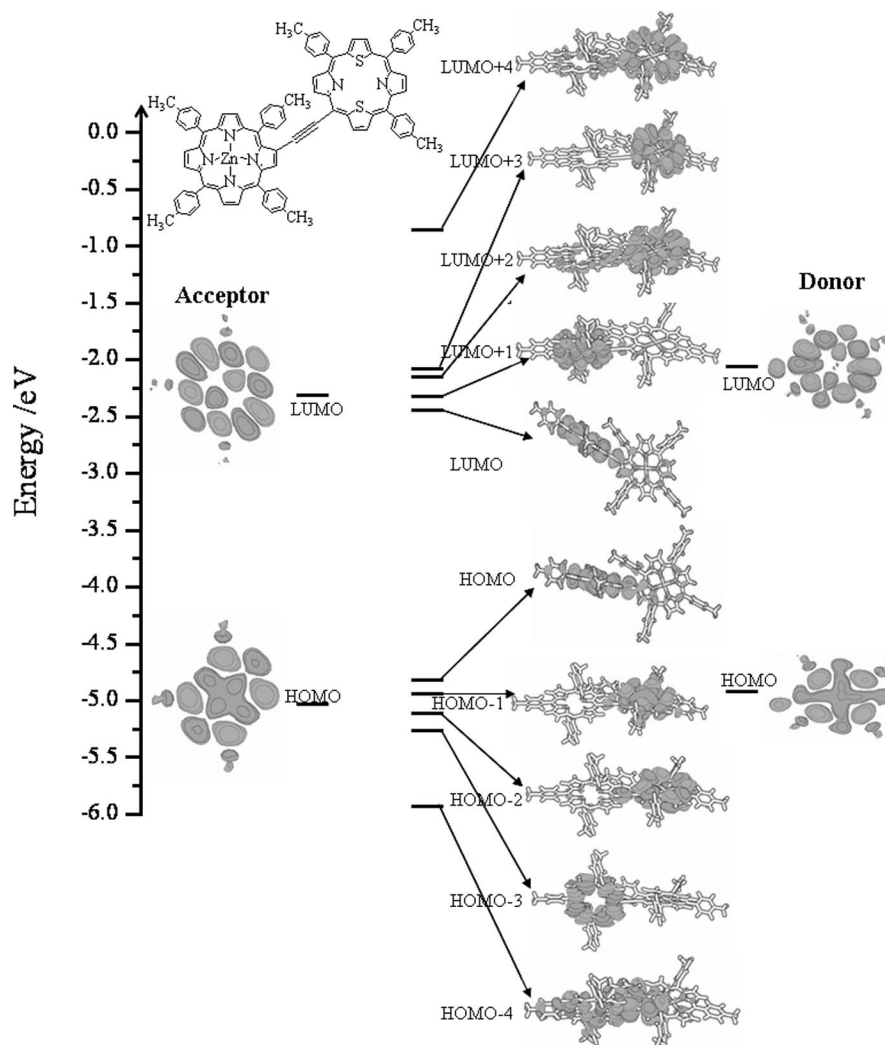


Figure 13. Frontier orbital correlation diagram for β ,*meso*, $\text{ZnN}_4\text{-N}_2\text{S}_2$, asymmetrical dyad **6**.

TOF Micromass spectrometer. The fluorescence quantum yields (Φ_f) of all the compounds were estimated from the emission and absorption spectra by a comparative method using H_2TTP ($\Phi_f = 0.11$) or ZnTPP ($\Phi_f = 0.033$) as reference compounds. MALDI-TOF spectra were obtained with an Axima-CFR instrument manufactured by Kratos Analyticals. CV and differential pulse voltammetric (DPV) studies were carried out with a BAS electrochemical system utilizing the three-electrode configuration, consisting of a glassy carbon (working) electrode, a platinum wire (auxiliary) electrode and a saturated calomel (reference) electrode. These experiments were performed in dry CH_2Cl_2 using 0.1 M tetrabutylammonium perchlorate as the supporting electrolyte. Under these conditions, ferrocene shows a reversible, one-electron oxidation wave ($E_{1/2} = 0.42$ V). The solution was degassed by purging with argon, and during the acquisition, argon was slowly passed over the solution. All general chemicals and solvents were procured from S. D. Fine Chemicals, India. Column chromatography was performed using silica gel obtained from Sisco Research Laboratories, India. Tetrabutylammonium perchlorate was purchased from Fluka and used without further purification. All other chemicals used for synthesis were reagent grade, unless otherwise specified.

Quantum-Chemical Methods: DFT calculations were carried out on the four dyads (**1**, **2**, **4** and **6**) shown in Figure 1 and their subunits

to determine their equilibrium structures and their electronic properties. A search for minimum energy structures was performed in the ground electronic state (S_0), applying Becke's three-parameter, correlated, hybrid, density functional (B3LYP) with 6-31G(d) atomic basis functions, which include ca. 3200 primitive Gaussian functions in total. Equilibrium structures of these systems were calculated based on a full geometry optimization without any symmetry restrictions according to the Newton–Raphson procedure. All these calculations were carried out with the GAMESS suite of programs for ab initio, electronic, structure calculations with a LINUX cluster platform.^[19] The visualization of molecular structures and orbital contour plots were carried out using MOLDEN visualization software.^[20]

[2-((3-Hydroxy-3-methylbut-1-yn-1-yl))-5,10,15,20-tetra(*p*-tolyl)porphyrinato]zinc(II) (9**):** To a deoxygenated solution of [2-bromo-5,10,15,20-tetra(*p*-tolyl)porphyrinato]zinc(II) (**8**, 200.0 mg, 0.25 mmol) in dry Et_3N /dimethylformamide (55 mL, 10:1), bis(triphenylphosphane)palladium(II) chloride (17.0 mg, 0.025 mmol), cuprous iodide (4.0 mg, 0.25 mmol) and 2-methyl-3-butyn-2-ol (238 μL , 2.5 mmol) were added. The reaction mixture was heated at reflux for 16 h, cooled and filtered through a short silica column using CH_2Cl_2 as the eluent. The solvent was removed under reduced pressure, and the crude residue was purified by silica gel

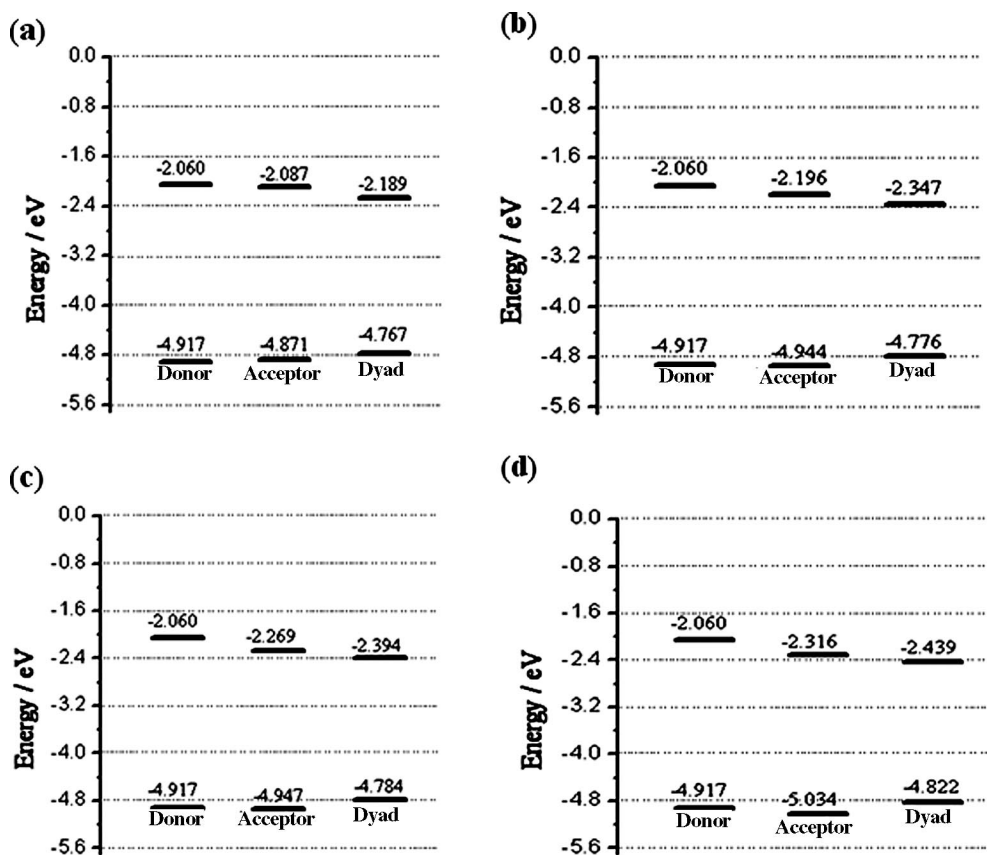


Figure 14. Pictorial representation of Kohn–Sham HOMO and LUMO energy levels of the four dyads (a) **1**, (b) **2**, (c) **4** and (d) **6** and the corresponding donor and acceptor macrocycles.

Table 5. HOMO and LUMO energy levels of dyads **1**, **2**, **4** and **6** and their corresponding monomers **10** and **16–19**.

Entry	System	ϵ_{HOMO} [eV]	ϵ_{LUMO} [eV]	$\epsilon_{\text{HOMO}} - \epsilon_{\text{LUMO}}$ [eV]
1	10	-4.92	-2.06	2.86
2	16	-4.87	-2.09	2.78
3	17	-4.94	-2.19	2.75
4	18	-4.95	-2.27	2.68
5	19	-5.03	-2.31	2.72
6	1	-4.77	-2.19	2.58
7	2	-4.78	-2.35	2.43
8	4	-4.78	-2.39	2.39
9	6	-4.82	-2.44	2.38

column chromatography. Pure **9** was collected with petroleum ether/ CH_2Cl_2 (20:80) and was obtained as a purple solid (148 mg, 63%). M.p. > 300 °C. ^1H NMR (400 MHz, CDCl_3): δ = 1.51 (s, 6 H, C- CH_3), 2.72 (s, 12 H, tolyl), 7.53–7.57 (m, 8 H, aryl), 8.05–8.08 (m, 8 H, aryl), 8.72 (d, J = 4.6 Hz, 1 H, β -pyrrole), 8.88 (d, J = 4.6 Hz, 1 H, β -pyrrole), 8.91–8.92 (m, 4 H, β -pyrrole), 9.13 (s, 1 H, β -pyrrole) ppm. ^{13}C NMR (100 MHz, CDCl_3): δ = 21.8, 29.9, 31.2, 65.7, 79.0, 103.2, 120.5, 120.9, 121.3, 121.6, 125.3, 127.4, 127.5, 131.9, 132.4, 132.7, 134.6, 134.8, 137.3, 137.6, 139.0, 139.9, 140.5, 147.2, 148.4, 150.4, 150.9, 151.0, 151.3 ppm. UV/Vis (toluene): λ (log ϵ) = 431 (5.73), 559 (4.24), 597 (3.65) nm. ESI-MS: m/z = 814.2 $[\text{M}]^+$. IR (KBr film): $\tilde{\nu}$ = 3328 (NH), 2966, 2853, 1966, 1464, 1268, 960, 802, 656 cm^{-1} . $\text{C}_{53}\text{H}_{42}\text{N}_4\text{OZn}$ (814.2): calcd. C 77.98, H 5.19, N 6.86; found C 77.86, H 5.25, N 6.90.

[2-Ethynyl-5,10,15,20-tetra(*p*-tolyl)porphyrinato]zinc(II) (10**):** Compound **9** (100.0 mg, 0.13 mmol) was dissolved in dry benzene

(90 mL) in a round-bottomed flask fitted with a Dean–Stark apparatus and reflux condenser. Potassium hydroxide (90 mg, 1.6 mmol), dissolved in CH_3OH (30 mL), was added to it, and the reaction mixture was stirred at 80 °C for 20 h. The solvent mixture collected in the Dean–Stark apparatus was removed at regular intervals, and the progress of the reaction was monitored by TLC analysis. The crude compound was subjected to silica gel column chromatography using petroleum ether/ CH_2Cl_2 (60:40) and afforded pure **10** as a purple crystalline solid (88 mg, 95%). M.p. > 300 °C. ^1H NMR (400 MHz, CDCl_3): δ = 2.70 (s, 12 H, tolyl), 3.27 (s, 1 H, CC-H), 7.45 (d, J = 7.9 Hz, 2 H, aryl), 7.53–7.55 (m, 6 H, aryl), 7.95 (d, J = 7.9 Hz, 2 H, aryl), 8.05–8.08 (m, 6 H, aryl), 8.90 (s, 2 H, β -pyrrole), 8.92 (s, 2 H, β -pyrrole), 8.94 (s, 2 H, β -pyrrole), 9.22 (s, 1 H, β -pyrrole) ppm. ^{13}C NMR (100 MHz, CDCl_3): δ = 21.8, 31.4, 78.9, 85.5, 121.2, 121.3, 121.4, 121.7, 124.8, 126.6, 126.8, 127.8, 127.9, 128.1, 132.0, 132.4, 132.5, 132.6, 133.0, 134.0, 134.6, 139.6, 142.7, 142.8, 148.0, 148.1, 150.9, 151.0 ppm. ESI-MS: m/z = 757.3 $[\text{M} + \text{H}]^+$. IR (KBr film): $\tilde{\nu}$ = 2926, 2850, 1966, 1645, 1464, 960, 800, 656 cm^{-1} . $\text{C}_{50}\text{H}_{36}\text{N}_4\text{Zn}$ (756.3): calcd. C 79.20, H 4.79, N 7.39; found C 79.32, H 4.81, N 7.26.

5-Bromo-10,15,20-tri(*p*-tolyl)-21-oxa-23-thiaporphyrin (14**):** To a stirred solution of 10,15,20-tri(*p*-tolyl)-21-oxa-23-thiaporphyrin (**18**, 40.0 mg, 0.066 mmol) in CHCl_3 (15 mL) was added NBS (12.0 mg, 0.066 mmol), and the mixture was stirred at room temperature for 20 min. The crude compound was subjected to silica gel column chromatography using petroleum ether/ CH_2Cl_2 (30:70) as the eluent and afforded the pure bromoporphyrin **14** as a purple solid (30 mg, 66%). M.p. > 300 °C. ^1H NMR (400 MHz, CDCl_3): δ = 2.7 (s, 9 H, 3 CH_3), 7.30–7.64 (m, 6 H, aryl), 8.03–8.10 (m, 6

H, aryl), 8.37 (d, $J = 4.6$ Hz, 1 H, β-pyrrole), 8.52 (d, $J = 4.6$ Hz, 1 H, β-pyrrole) 8.64 (d, $J = 4.6$ Hz, 1 H, β-pyrrole), 9.35 (d, $J = 4.6$ Hz, 1 H, β-furan), 9.37 (d, $J = 4.6$ Hz, 1 H, β-pyrrole), 9.65 (s, 1 H, β-furan), 9.66 (d, $J = 5.2$ Hz, 1 H, β-thiophene), 10.15 (d, $J = 5.2$ Hz, 1 H, β-thiophene) ppm. ^{13}C NMR (100 MHz, CDCl_3): $\delta = 21.7, 110.2, 114.0, 128.4, 128.5, 134.3, 134.7, 135.2, 135.9, 136.1, 136.3, 138.1, 138.4, 145.8, 148.3, 148.7, 156.8, 157.1, 157.3$ ppm. ESI-MS: $m/z = 677.1/679.1$ [$\text{M} + 1$] $^+$ ($\text{Br}^{79}/\text{Br}^{81}$). IR (KBr film): $\tilde{\nu} = 2923, 2835, 1966, 1645, 1464, 960, 800, 645$ cm^{-1} . $\text{C}_{41}\text{H}_{33}\text{BrN}_2\text{OS}$ (676.1): calcd. C 72.67, H 4.31, N 4.13; found C 72.75, H 4.25, N 4.26.

5-Bromo-10,15,20-tri(*p*-tolyl)-21,23-dithiaporphyrin (15): Compound **15** was prepared under similar reaction conditions as described above for **14** by treating 10,15,20-tri(*p*-tolyl)-21,23-dithiaporphyrin (**19**, 55.0 mg, 0.0901 mmol) in CHCl_3 (15 mL) at room temperature with NBS (16.0 mg, 0.0901 mmol) at room temperature for 10 min. The progress of the reaction was monitored by TLC analysis. After completion of the reaction, acetone/ CH_3OH (10 mL, 1:1) was added to quench the reaction. The solvent was removed in a rotary evaporator under reduced pressure, and the crude reaction mixture was purified by silica gel column chromatography using petroleum ether/ CH_2Cl_2 (90:10) as the eluent. The desired bromoporphyrin **15** was obtained as a purple solid (58 mg, 93%). M.p. > 300 °C. ^1H NMR (400 MHz, CDCl_3): $\delta = 2.7$ (s, 9 H, 3 CH_3), 7.58–7.63 (m, 6 H, aryl), 8.07–8.11 (m, 6 H, aryl), 8.64 (s, 2 H, β-pyrrole), 8.70 (d, $J = 4.6$ Hz, 1 H, β-pyrrole), 9.31 (d, $J = 4.6$ Hz, 1 H, β-pyrrole), 9.64 (s, 2 H, β-thiophene), 9.76 (d, $J = 5.2$ Hz, 1 H, β-thiophene), 10.20 (d, $J = 5.2$ Hz, 1 H, β-thiophene) ppm. ^{13}C NMR (100 MHz, CDCl_3): $\delta = 21.7, 110.2, 114.0, 128.4, 128.5, 134.3, 134.7, 135.2, 135.9, 136.1, 136.3, 138.1, 138.4, 145.8, 148.3, 148.7, 156.8, 157.1, 157.3$ ppm. ESI-MS: $m/z = 694.2/696.3$ [$\text{M} + 1$] $^+$ ($\text{Br}^{79}/\text{Br}^{81}$). IR (KBr film): $\tilde{\nu} = 2931, 2855, 1935, 1643, 1461, 964, 805$ cm^{-1} . $\text{C}_{41}\text{H}_{29}\text{BrN}_2\text{S}_2$ (693.2): calcd. C 70.99, H 4.21, N 4.04; found C 71.05, H 4.18, N 4.09.

General Procedure for the Synthesis of Asymmetrical, β,meso-Ethynyl-Bridged ZnN_4 Porphyrin-Heteroporphyrin Dyads 1, 2, 4 and 6: meso-Bromoporphyrin and [2-ethynyl-5,10,15,20-tetra(*p*-tolyl)porphyrinato]zinc(II) were dissolved in dry toluene/ Et_3N (6 mL, 5:1) in a 25 mL, two-necked, round-bottomed flask fitted with a reflux condenser, gas inlet and gas outlet tubes for nitrogen purging. The reaction vessel was placed in an oil bath preheated to 35 °C. After purging the flask with nitrogen for 15 min, AsPh_3 (3.5 equiv.) and $\text{Pd}_2(\text{dba})_3$ (0.44 equiv.) were added, and the reaction mixture was stirred at 35 °C for 4 h. TLC analysis of the reaction mixture indicated the appearance of a dark new spot apart from the faded, two starting monomeric porphyrin spots. The solvent was removed under reduced pressure, and the crude compound was purified by silica gel chromatography. The excess AsPh_3 and the small amounts of unreacted starting porphyrin building blocks were removed with petroleum ether/ CH_2Cl_2 , and the required pure dyad was then collected with CH_2Cl_2 .

[5,10,15,20-Tetra(*p*-tolyl)-2-{2-[10',15',20'-tri(*p*-tolyl)-21-oxaporphin-5'-yl]ethynyl}porphyrinato]zinc(II) (1): Yield: 57%. M.p. > 300 °C. ^1H NMR (400 MHz, CDCl_3): $\delta = 1.48$ (s, 3 H, CH_3), 2.62 (s, 3 H, CH_3), 2.69 (s, 6 H, 2 CH_3), 2.71 (s, 6 H, 2 CH_3), 2.72 (s, 3 H, CH_3), 6.80 (d, $J = 8.2$ Hz, 2 H, aryl), 7.51–7.72 (m, 12 H, aryl), 8.01–8.21 (m, 14 H, aryl), 8.65 (d, $J = 4.3$ Hz, 1 H, β-pyrrole), 8.78 (d, $J = 4.3$ Hz, 1 H, β-pyrrole), 8.82 (d, $J = 2.3$ Hz, 1 H, β-pyrrole), 8.89 (d, $J = 2.1$ Hz, 1 H, β-pyrrole), 8.95 (d, $J = 4.6$ Hz, 1 H, β-pyrrole), 8.97 (d, $J = 4.6$ Hz, 1 H, β-pyrrole), 8.98 (d, $J = 4.6$ Hz, 1 H, β-pyrrole), 9.00 (d, $J = 4.6$ Hz, 1 H, β-pyrrole), 9.22 (d, $J = 4.6$ Hz, 1 H, β-pyrrole), 9.33 (d, $J = 4.6$ Hz, 1 H, β-furan), 9.59 (d,

$J = 4.6$ Hz, 1 H, β-pyrrole), 9.62–9.63 (m, 2 H, β-furan and β-pyrrole), 9.68 (s, 1 H, β-pyrrole), 9.75 (d, $J = 3.9$ Hz, 1 H, β-pyrrole) ppm. ^{13}C NMR (100 MHz, CDCl_3): $\delta = 21.5, 21.7, 22.6, 65.2, 110.2, 121.5, 121.8, 127.5, 127.8, 128.5, 129.7, 130.5, 131.9, 132.4, 132.6, 133.0, 133.8, 134.0, 134.3, 134.7, 135.3, 136.8, 137.3, 137.5, 138.0, 138.3, 139.6, 140.0, 146.3, 147.9, 148.5, 150.4, 151.1, 151.2, 151.3, 151.7, 156.7, 157.9, 158.8$ ppm. MALDI-TOF-MS: $m/z = 1335.2$ [M] $^+$. IR (KBr film): $\tilde{\nu} = 3046, 2914, 2840, 2211, 1641, 1458, 967, 820, 654$ cm^{-1} .

[5,10,15,20-Tetra(*p*-tolyl)-2-{2-[10',15',20'-tri(*p*-tolyl)-21-thiaporphin-5'-yl]ethynyl}porphyrinato]zinc(II) (2): Yield: 84%. M.p. > 300 °C. ^1H NMR (400 MHz, CDCl_3): $\delta = -2.10$ (s, 1 H, NH), 1.50 (s, 3 H, CH_3), 2.65 (s, 3 H, CH_3), 2.69 (s, 6 H, 2 CH_3), 2.70 (s, 6 H, 2 CH_3), 2.72 (s, 3 H, CH_3), 6.83 (d, $J = 8.2$ Hz, 2 H, aryl), 7.56–7.72 (m, 12 H, aryl), 8.06–8.21 (m, 14 H, aryl), 8.56 (d, $J = 4.6$ Hz, 1 H, β-pyrrole), 8.58 (d, $J = 4.6$ Hz, 1 H, β-pyrrole), 8.65 (d, $J = 4.6$ Hz, 1 H, β-pyrrole), 8.88 (d, $J = 2.1$ Hz, 2 H, β-pyrrole), 8.90 (s, 2 H, β-pyrrole), 8.96 (s, 2 H, β-pyrrole), 8.99 (d, $J = 4.6$ Hz, 1 H, β-pyrrole), 9.03 (d, $J = 4.6$ Hz, 1 H, β-pyrrole), 9.24 (d, $J = 4.3$ Hz, 1 H, β-pyrrole), 9.62 (s, 1 H, β-pyrrole), 9.76 (d, $J = 4.9$ Hz, 1 H, β-thiophene), 10.20 (d, $J = 4.9$ Hz, 1 H, β-thiophene) ppm. ^{13}C NMR (100 MHz, CDCl_3): $\delta = 21.5, 22.7, 23.0, 23.7, 68.1, 112.1, 121.1, 121.4, 124.4, 124.9, 125.9, 127.3, 127.6, 128.4, 128.9, 130.9, 131.0, 131.8, 132.4, 132.9, 133.6, 134.1, 134.3, 134.7, 135.2, 135.5, 137.1, 137.5, 137.9, 138.4, 138.7, 138.9, 139.3, 139.5, 139.8, 143.3, 146.5, 148.1, 148.4, 148.9, 150.3, 150.9, 151.2, 157.6, 158.9$ ppm. MALDI-TOF-MS: $m/z = 1351.3$ [M] $^+$. IR (KBr film): $\tilde{\nu} = 3025, 2920, 2841, 2315, 1670, 1460, 967, 812, 650$ cm^{-1} .

[5,10,15,20-Tetra(*p*-tolyl)-2-{2-[10',15',20'-tri(*p*-tolyl)-21-oxa-23-thiaporphin-5'-yl]ethynyl}porphyrinato]zinc(II) (4): Yield: 69%. M.p. > 300 °C. ^1H NMR (400 MHz, CDCl_3): $\delta = 1.56$ (s, 3 H, CH_3), 2.66 (s, 3 H, CH_3), 2.70 (s, 12 H, 4 CH_3), 2.73 (s, 3 H, CH_3), 6.96 (d, $J = 7.3$ Hz, 2 H, aryl), 7.51–7.65 (m, 12 H, aryl), 8.07–8.24 (m, 14 H, aryl), 8.37 (d, $J = 4.3$ Hz, 1 H, β-pyrrole), 8.52 (d, $J = 4.3$ Hz, 1 H, β-pyrrole), 8.60 (d, $J = 4.3$ Hz, 1 H, β-pyrrole), 8.85 (d, $J = 1.3$ Hz, 1 H, β-pyrrole), 8.89 (d, $J = 1.3$ Hz, 1 H, β-pyrrole), 8.95 (d, $J = 1.3$ Hz, 2 H, β-pyrrole), 8.98 (d, $J = 4.6$ Hz, 1 H, β-pyrrole), 9.00 (d, $J = 4.6$ Hz, 1 H, β-pyrrole), 9.22 (d, $J = 4.6$ Hz, 1 H, β-pyrrole), 9.33 (d, $J = 4.6$ Hz, 1 H, β-furan), 9.63 (m, 2 H, β-furan and β-pyrrole), 9.64 (s, 1 H, β-thiophene), 9.96 (d, $J = 4.0$ Hz, 1 H, β-thiophene) ppm. ^{13}C NMR (100 MHz, CDCl_3): $\delta = 20.5, 21.7, 22.8, 52.2, 110.2, 121.5, 121.6, 127.5, 127.8, 128.5, 129.7, 130.5, 131.9, 132.4, 132.6, 133.0, 133.8, 134.0, 134.3, 134.7, 135.3, 136.8, 137.3, 137.5, 138.0, 138.3, 139.6, 140.0, 146.3, 147.9, 148.5, 150.4, 151.1, 151.2, 151.3, 151.7, 156.7, 157.9, 158.8$ ppm. MALDI-TOF-MS: $m/z = 1352.6$ [M] $^+$. IR (KBr film): $\tilde{\nu} = 3033, 2915, 2839, 2223, 1665, 1458, 970, 821, 651$ cm^{-1} .

[5,10,15,20-Tetra(*p*-tolyl)-2-{2-[10',15',20'-tri(*p*-tolyl)-21,23-dithiaporphin-5'-yl]ethynyl}porphyrinato]zinc(II) (6): Yield: 88%. M.p. > 300 °C. ^1H NMR (400 MHz, CDCl_3): $\delta = 1.34$ (s, 3 H, CH_3), 2.66 (s, 3 H, CH_3), 2.70 (s, 6 H, 2 CH_3), 2.71 (s, 6 H, 2 CH_3), 2.73 (s, 3 H, CH_3), 6.83 (d, $J = 8.2$ Hz, 2 H, aryl), 7.53–7.65 (m, 12 H, aryl), 8.09–8.22 (m, 14 H, aryl), 8.65 (s, 2 H, β-pyrrole), 8.67 (d, $J = 4.6$ Hz, 1 H, β-pyrrole), 8.90 (s, 2 H, β-pyrrole), 8.95 (s, 2 H, β-pyrrole), 8.99 (d, $J = 4.9$ Hz, 1 H, β-pyrrole), 9.01 (d, $J = 4.9$ Hz, 1 H, β-pyrrole), 9.28 (d, $J = 4.6$ Hz, 1 H, β-pyrrole), 9.62 (s, 1 H, β-pyrrole), 9.63 (d, $J = 1.8$ Hz, 2 H, β-thiophene), 9.70 (d, $J = 4.9$ Hz, 1 H, β-thiophene), 10.20 (d, $J = 4.9$ Hz, 1 H, β-thiophene) ppm. ^{13}C NMR (100 MHz, CDCl_3): $\delta = 21.7, 22.8, 23.1, 23.9, 68.3, 115.0, 121.3, 121.6, 125.9, 127.5, 127.8, 128.4, 128.9, 131.0, 131.9, 132.4, 132.6, 133.0, 133.7, 134.3, 134.6, 135.0, 135.5, 137.3, 137.5, 138.0, 138.3, 138.5, 138.7, 138.9, 139.5, 140.0, 147.4, 148.0, 148.4,$

149.4, 150.4, 151.1, 151.2, 156.2, 156.5, 157.0, 158.2 ppm. MALDI-TOF-MS: $m/z = 1367.2$ [M]⁺. IR (KBr film): $\tilde{\nu} = 3033, 2920, 2845, 2309, 1656, 1462, 974, 811, 641$ cm⁻¹.

General Procedure for the Synthesis of Asymmetrical, β ,*meso*-Ethylene-Bridged, N₄ Porphyrin–Heteroporphyrin Dyads 3, 5 and 7: The corresponding ZnN₄ porphyrin–heteroporphyrin dyads 2, 4 and 6 in CH₂Cl₂ were treated with excess TFA for 15 min. The progress of the reaction was monitored by absorption spectroscopy. After the standard workup, the crude compounds were purified by silica gel column chromatography using CH₂Cl₂, and they afforded pure N₄ porphyrin–heteroporphyrin dyads 3, 5 and 7, respectively, in ca. 90% yields.

1-[5,10,15,20-Tetra(*p*-tolyl)porphin-2-yl]-2-[10',15',20'-tri(*p*-tolyl)-21-thiaporphin-5'-yl]ethyne (3): Yield: 94%. M.p. > 300 °C. ¹H NMR (400 MHz, CDCl₃): $\delta = -2.56$ (s, 2 H, NH), -2.12 (s, 1 H, NH), 1.42 (s, 3 H, CH₃), 2.66 (s, 3 H, CH₃), 2.69 (s, 6 H, 2 CH₃), 2.71 (s, 6 H, 2 CH₃), 2.73 (s, 3 H, CH₃), 6.86 (d, $J = 7.6$ Hz, 2 H, aryl), 7.54 – 7.65 (m, 12 H, aryl), 8.05 – 8.22 (m, 14 H, aryl), 8.56 (d, $J = 4.6$ Hz, 1 H, β -pyrrole), 8.58 (d, $J = 4.6$ Hz, 1 H, β -pyrrole), 8.63 (d, $J = 4.6$ Hz, 1 H, β -pyrrole), 8.81 (s, 2 H, β -pyrrole), 8.87 (s, 4 H, β -pyrrole), 8.94 (d, $J = 4.6$ Hz, 1 H, β -pyrrole), 8.99 (d, $J = 4.6$ Hz, 1 H, β -pyrrole), 9.22 (d, $J = 4.3$ Hz, 1 H, β -pyrrole), 9.46 (s, 1 H, β -pyrrole), 9.75 (d, $J = 5.2$ Hz, 1 H, β -thiophene), 10.16 (d, $J = 5.2$ Hz, 1 H, β -thiophene) ppm. ¹³C NMR (100 MHz, CDCl₃): $\delta = 21.3, 22.6, 23.5, 23.7, 67.5, 112.6, 121.1, 121.4, 124.4, 124.9, 125.9, 127.5, 127.6, 128.4, 128.9, 130.9, 131.6, 131.8, 132.4, 132.9, 133.6, 134.1, 134.3, 134.7, 135.2, 135.5, 137.1, 137.5, 137.9, 138.4, 138.7, 138.9, 139.3, 139.5, 139.8, 143.3, 146.5, 148.1, 148.4, 148.9, 150.3, 150.9, 151.4, 157.6, 158.6$ ppm. MALDI-TOF-MS: $m/z = 1289.5$ [M + H]⁺. IR (KBr film): $\tilde{\nu} = 3031, 2925, 2860, 2212, 1641, 1458, 966, 822, 656$ cm⁻¹.

1-[5,10,15,20-Tetra(*p*-tolyl)porphin-2-yl]-2-[10',15',20'-tri(*p*-tolyl)-21-oxa-23-thiaporphin-5'-yl]ethyne (5): Yield: 90%. M.p. > 300 °C. ¹H NMR (400 MHz, CDCl₃): $\delta = -2.55$ (s, 2 H, NH), 1.45 (s, 3 H, CH₃), 2.66 (s, 3 H, CH₃), 2.70 (s, 12 H, 4 CH₃), 2.73 (s, 3 H, CH₃), 6.98 (d, $J = 7.0$ Hz, 2 H, aryl), 7.51 – 7.64 (m, 12 H, aryl), 8.06 – 8.25 (m, 14 H, aryl), 8.35 (d, $J = 4.3$ Hz, 1 H, β -pyrrole), 8.52 (d, $J = 4.3$ Hz, 1 H, β -pyrrole), 8.60 (d, $J = 3.9$ Hz, 1 H, β -pyrrole), 8.81 – 8.95 (m, 6 H, β -pyrrole), 9.20 (d, $J = 3.9$ Hz, 1 H, β -pyrrole), 9.30 (d, $J = 4.3$ Hz, 1 H, β -furan), 9.48 (s, 1 H, β -pyrrole), 9.63 – 9.64 (m, 2 H, β -furan and β -thia), 9.92 (d, $J = 4.8$ Hz, 1 H, β -thiophene) ppm. ¹³C NMR (100 MHz, CDCl₃): $\delta = 21.2, 21.7, 22.8, 52.6, 110.2, 121.5, 121.9, 127.5, 127.8, 128.5, 129.7, 130.5, 131.9, 132.4, 132.6, 133.0, 133.8, 134.0, 134.3, 134.7, 135.3, 136.8, 137.3, 137.5, 138.0, 138.3, 139.6, 140.0, 146.3, 147.7, 148.5, 150.4, 151.1, 151.2, 151.3, 151.7, 157.1, 157.9, 158.6$ ppm. MALDI-TOF-MS: $m/z = 1290.6$ [M + H]⁺. IR (KBr film): $\tilde{\nu} = 3046, 2915, 2840, 2211, 1641, 1458, 967, 820, 654$ cm⁻¹.

1-[5,10,15,20-Tetra(*p*-tolyl)porphin-2-yl]-2-[10',15',20'-tri(*p*-tolyl)-21,23-dithiaporphin-5'-yl]ethyne (7): Yield: 96%. M.p. > 300 °C. ¹H NMR (400 MHz, CDCl₃): $\delta = -2.56$ (s, 1 H, NH), 1.42 (s, 3 H, CH₃), 2.66 (s, 3 H, CH₃), 2.70 (s, 6 H, 2 CH₃), 2.72 (s, 6 H, 2 CH₃), 2.73 (s, 3 H, CH₃), 6.84 (d, $J = 7.6$ Hz, 2 H, aryl), 7.52 – 7.65 (m, 12 H, aryl), 8.11 – 8.23 (m, 14 H, aryl), 8.65 (s, 2 H, β -pyrrole), 8.66 (d, $J = 4.6$ Hz, 1 H, β -pyrrole), 8.81 (d, $J = 1.6$ Hz, 2 H, β -pyrrole), 8.87 (s, 2 H, β -pyrrole), 8.96 (d, $J = 4.6$ Hz, 1 H, β -pyrrole), 8.98 (d, $J = 4.6$ Hz, 1 H, β -pyrrole), 9.25 (d, $J = 4.6$ Hz, 1 H, β -pyrrole), 9.47 (s, 1 H, β -pyrrole), 9.63 (d, $J = 1.5$ Hz, 2 H, β -thiophene), 9.70 (d, $J = 5.2$ Hz, 1 H, β -thiophene), 10.17 (d, $J = 5.2$ Hz, 1 H, β -thiophene) ppm. ¹³C NMR (100 MHz, CDCl₃): $\delta = 21.1, 22.6, 23.15, 23.9, 68.3, 115.0, 121.6, 121.6, 125.9, 127.6, 127.8, 128.4, 128.9, 131.5, 131.9, 132.4, 132.6, 133.0, 133.7, 134.3, 134.6, 135.0,$

$135.5, 137.3, 137.5, 138.0, 138.4, 138.5, 138.7, 138.9, 139.5, 140.0, 147.3, 148.0, 148.4, 149.4, 150.4, 151.1, 151.2, 156.2, 156.5, 157.5, 159.0$ ppm. MALDI-TOF-MS: $m/z = 1306.5$ [M + H]⁺. IR (KBr film): $\tilde{\nu} = 3045, 2915, 2842, 2211, 1641, 1456, 967, 822, 653$ cm⁻¹.

Supporting Information (see footnote on the first page of this article): NMR, MS and Cartesian coordinates of selected compounds.

Acknowledgments

M. R. thanks the Council of Scientific and Industrial Research (CSIR) and the Department of Science and Technology (DST) for financial support, and Y. K. thanks CSIR for a fellowship. The Computer Centre, Bhabha Atomic Research Centre (BARC) is gratefully acknowledged for generous CPU time on their ANU-PAM, parallel, computer systems.

- [1] a) S. Gaspard, C. Giannotti, P. Maillard, C. Schaeffer, T. H. T. Thi, *J. Chem. Soc., Chem. Commun.* **1986**, 1239–1241; b) H. J. Tian, Q. F. Zhou, S. Y. Shen, H. J. Xu, *J. Photochem. Photobiol. A: Chem.* **1993**, *72*, 163–168; c) L. Li, S. Shen, Q. Yu, Q. Zhou, H. Xu, *J. Chem. Soc., Chem. Commun.* **1991**, 619–620.
- [2] a) R. Paolesse, R. K. Pandey, T. P. Forsyth, L. Jaquinod, K. R. Gerzevske, D. J. Nurco, M. O. Senge, S. Licocchia, T. Boschi, K. M. Smith, *J. Am. Chem. Soc.* **1996**, *118*, 3869–3882; b) M. R. Wasielewski, D. G. Johnson, M. P. Niemczyk, G. L. Gaines III, M. P. O'Neil, W. A. Svec, *J. Am. Chem. Soc.* **1990**, *112*, 6482–6488; c) G. Zheng, R. K. Pandey, T. P. Forsyth, A. N. Kozyrev, T. J. Dougherty, K. M. Smith, *Tetrahedron Lett.* **1997**, *38*, 2409–2412; d) D. P. Arnold, R. D. Hartnell, *Tetrahedron Lett.* **2001**, *57*, 1335–1345; e) A. R. Genady, D. Gabel, *Tetrahedron Lett.* **2003**, *44*, 2915–2917.
- [3] a) R. Paolesse, F. Sagone, A. Macagnano, T. Boschi, L. Prodi, M. Montalti, N. Zaccaroni, F. Bolletta, K. M. Smith, *J. Porphyrins Phthalocyanines* **1999**, *3*, 364–370; b) R. Guilard, C. P. Gros, J. M. Barbe, E. Espinosa, F. Jerome, A. Tabard, *Inorg. Chem.* **2004**, *43*, 7441–7455; c) K. M. Kadish, L. Fremont, Z. Ou, J. Shao, C. Shi, F. C. Anson, F. Burdet, C. P. Gros, J. M. Barbe, R. Guilard, *J. Am. Chem. Soc.* **2005**, *127*, 5625–5631; d) J. M. Barbe, F. Burdet, E. Espinosa, R. Guilard, *Eur. J. Inorg. Chem.* **2005**, 1032–1041; e) L. Flamigni, B. Ventura, M. Tasiar, D. T. Gryko, *Inorg. Chim. Acta* **2007**, *360*, 803–813.
- [4] a) R. P. Pandian, T. K. Chandrashekar, *Inorg. Chem.* **1994**, *33*, 3311–3324; b) I. Gupta, N. Agarwal, M. Ravikanth, *Eur. J. Org. Chem.* **2004**, 1693–1697; c) I. Gupta, M. Ravikanth, *J. Org. Chem.* **2004**, *69*, 6796–6811; d) S. Punidha, N. Agarwal, M. Ravikanth, *Eur. J. Org. Chem.* **2005**, 2500–2517; e) I. Gupta, M. Ravikanth, *Inorg. Chim. Acta* **2007**, *360*, 1731–1742; f) S. Punidha, J. Sinha, A. Kumar, M. Ravikanth, *J. Org. Chem.* **2008**, *73*, 323–328.
- [5] a) J. S. Hsiao, B. P. Krueger, R. W. Wagner, T. E. Johnson, J. K. Delaney, D. C. Mauzerall, G. R. Fleming, J. S. Lindsey, D. F. Bocian, R. J. Donohoe, *J. Am. Chem. Soc.* **1996**, *118*, 11181–11193; b) D. Holten, D. F. Bocian, J. S. Lindsey, *Acc. Chem. Res.* **2002**, *35*, 57–69; c) R. W. Wagner, T. E. Johnson, F. Li, J. S. Lindsey, *J. Org. Chem.* **1995**, *60*, 5266–5273; d) F. Li, S.-I. Yang, Y. Ciringh, J. Seth, C. H. Martin, D. L. Singh, D. Kim, R. R. Birge, D. F. Bocian, D. Holten, J. S. Lindsey, *J. Am. Chem. Soc.* **1998**, *120*, 10001–10017; e) L. Karki, F. W. Vance, J. T. Hupp, L. S. M. Cours, M. J. Therien, *J. Am. Chem. Soc.* **1998**, *120*, 2606–2611; f) A. K. Burrell, D. L. Officer, D. C. W. Reid, K. Y. Wild, *Angew. Chem. Int. Ed.* **1998**, *37*, 114–117; g) A. K. Burrell, D. L. Officer, P. G. Plieger, D. C. Reid, *Chem. Rev.* **2001**, *101*, 2751–2796; h) N. Yoshida, T. Ishizuka, K. Youfu, M. Murakami, H. Miyasaka, T. Okada, Y. Nagata, A. Itaya, H. S. Cho, D. Kim, A. Osuka, *Chem. Eur. J.* **2003**, *9*, 2854–2866; i) A. Osuka, D. Fujikane, H. Shimori, S. Kobayake, M. Irie, *J. Org. Chem.* **2001**, *66*, 3913–3923; j) C. C. Mak,

- N. Bampos, J. K. M. Sanders, *Angew. Chem. Int. Ed.* **1998**, *37*, 3020–3023; k) D. Kuciauskas, P. A. Liddell, S. Lin, T. E. Johnson, J. S. Weghorn, J. S. Lindsey, A. L. Moore, T. A. Moore, D. Gust, *J. Am. Chem. Soc.* **1999**, *121*, 8604–8614; l) O. Mongin, C. Papamicael, N. Hoyer, A. Gossauer, *J. Org. Chem.* **1998**, *63*, 5568–5580; m) R. Paolesse, L. Jaquinod, F. D. Sala, D. J. Nurco, L. Prodi, M. Montalti, C. D. Natale, A. D'Amico, D. A. Carlo, P. Lugli, K. M. Smith, *J. Am. Chem. Soc.* **2000**, *122*, 11295–11302; n) R. Beavington, P. L. Burn, *J. Chem. Soc. Perkin Trans. 1* **2000**, 1231–1240; o) K.-I. Sugiura, T. Matsumoto, S. Ohkouchi, Y. Naitoh, T. Kawai, Y. Takai, K. Ushiroda, Y. Sakata, *Chem. Commun.* **1999**, 1957–1958; p) M. J. Crossley, P. Thordarson, *Angew. Chem. Int. Ed.* **2002**, *41*, 1709–1712; q) M. J. Crossley, L. A. Johnston, *Chem. Commun.* **2002**, 1122–1123; r) A. Vidal-Ferran, Z. Clyde-Waston, N. Bampos, J. K. M. Sanders, *J. Org. Chem.* **1997**, *62*, 240–241.
- [6] a) S. I. Yang, J. Li, H. S. Cho, D. Kim, D. F. Bocian, D. Holten, J. S. Lindsey, *J. Mater. Chem.* **2000**, *10*, 283–296; b) J. Li, J. R. Dires, J. Seth, S. I. Yang, D. F. Bocian, D. Holten, J. S. Lindsey, *J. Org. Chem.* **1999**, *64*, 9090–9100; c) J. Li, J. S. Lindsey, *J. Org. Chem.* **1999**, *64*, 9101–9108.
- [7] I. Gupta, M. Ravikanth, *Coord. Chem. Rev.* **2006**, *250*, 468–518 and references cited therein.
- [8] H. Shinokubo, A. Osuka, *Chem. Commun.* **2009**, 1011–1021 and references cited therein.
- [9] a) V. S.-Y. Lin, S. G. DiMaggio, M. J. Therien, *Science* **1994**, *264*, 1105–1111; b) P. J. Angiolillo, V. S.-Y. Lin, J. M. Vanderkooi, M. J. Therien, *J. Am. Chem. Soc.* **1995**, *117*, 12514–12527; c) R. Kumble, S. Palese, V. S.-Y. Lin, M. J. Therien, R. M. Hochstrasser, *J. Am. Chem. Soc.* **1998**, *120*, 11489–11498; d) J. T. Fletcher, M. J. Therien, *J. Am. Chem. Soc.* **2000**, *122*, 12393–12394; e) R. Shediach, M. H. B. Gray, H. Tetsuo Uyeda, R. C. Johnson, J. T. Hupp, P. J. P. J. Angiolillo, M. J. Therien, *J. Am. Chem. Soc.* **2000**, *122*, 7017–7033; f) K. Susumu, T. V. Duncan, M. J. Therien, *J. Am. Chem. Soc.* **2005**, *127*, 5186–5195; g) K. Susumu, P. R. Frail, P. J. Angiolillo, M. J. Therien, *J. Am. Chem. Soc.* **2006**, *128*, 8380–8381; h) T. V. Duncan, P. Ghoroghchian, I. V. Rubtsov, D. A. Hammer, M. J. Therien, *J. Am. Chem. Soc.* **2008**, *130*, 9773–9784.
- [10] a) T. Nagata, A. Osuka, K. Maruyama, *J. Am. Chem. Soc.* **1990**, *112*, 3054–3059; b) M. Ikeda, S. Shinkai, A. Osuka, *Chem. Commun.* **2000**, 1047–1048; c) N. Aratani, A. Osuka, *Org. Lett.* **2001**, *3*, 4213–4216; d) A. Tsuda, A. Osuka, *Science* **2001**, *293*, 79–82; e) N. Aratani, H. S. Cho, T. K. Ahn, S. Cho, D. Kim, H. Sumi, A. Osuka, *J. Am. Chem. Soc.* **2003**, *125*, 9668–9681; f) N. Aratani, H. S. Cho, T. K. Ahn, S. Cho, D. Kim, H. Sumi, A. Osuka, *J. Am. Chem. Soc.* **2003**, *125*, 9668–9681; g) H. Hata, H. Shinokubo, A. Osuka, *J. Am. Chem. Soc.* **2005**, *127*, 8264–8265; h) H. Hata, S. Yamaguchi, G. Mori, S. Nakazono, T. Katoh, K. Takatsu, S. Hiroto, H. Shinokubo, A. Osuka, *Chem. Asian J.* **2007**, *2*, 849–859; i) I. Hisaki, S. Hiroto, K. S. Kim, S. B. Noh, D. Kim, H. Shinokubo, A. Osuka, *Angew. Chem. Int. Ed.* **2007**, *46*, 5125–5128; j) J. Song, S. Y. Jang, S. Yamaguchi, J. Sankar, S. Hiroto, N. Aratani, J.-Y. Shin, S. Easwaramoorthi, K. S. Kim, D. Kim, H. Shinokubo, A. Osuka, *Angew. Chem. Int. Ed.* **2008**, *47*, 6004–6007; k) N. Aratani, A. Osuka, *Chem. Commun.* **2008**, 4067–4069; l) J. Yang, M. Park, Z. S. Yoon, T. Hori, X. Peng, N. Aratani, P. Dedecker, J. Hotta, H. Uji-I, M. Sliwa, J. Hofkens, A. Osuka, D. Kim, *J. Am. Chem. Soc.* **2008**, *130*, 1879–1884.
- [11] a) X. Zhou, K. S. Chan, *J. Chem. Soc., Chem. Commun.* **1994**, 2493–2494; b) X. Zhou, K. S. Chan, *J. Org. Chem.* **1998**, *63*, 99–104; c) Y. Deng, C. K. Chang, D. G. Nocera, *Angew. Chem. Int. Ed.* **2000**, *39*, 1066–1068.
- [12] H. J. Callot, *Tetrahedron Lett.* **1973**, *14*, 4987–4990.
- [13] S. Punidha, N. Agarwal, R. Burai, M. Ravikanth, *Eur. J. Org. Chem.* **2004**, 2223–2230.
- [14] J. S. Lindsey, I. C. Schreiman, H. C. Hsu, P. C. Kearney, A. M. Marguerettaz, *J. Org. Chem.* **1987**, *52*, 827–836.
- [15] R. W. Wagner, T. E. Johnson, F. Li, J. S. Lindsey, *J. Org. Chem.* **1996**, *60*, 5266–5273.
- [16] a) G. Bringmann, D. C. G. Götz, T. A. M. Gulder, T. H. Gehrke, T. Bruhn, T. Kupfer, K. Radacki, H. Braunschweig, A. Heckmann, C. Lambert, *J. Am. Chem. Soc.* **2008**, *130*, 17812–17825; b) G. Bringmann, S. Rüdener, D. C. G. Götz, T. A. M. Gulder, M. Reichert, *Org. Lett.* **2006**, *8*, 4743–4746; c) A. Wiehe, M. O. Senge, A. Schäfer, M. Speck, S. Tannert, H. Kurreck, B. Röder, *Tetrahedron* **2001**, *57*, 10089–10110; d) M. O. Senge, B. Rössler, J. Von Gersdorff, A. Schäfer, H. Kurreck, *Tetrahedron Lett.* **2004**, *45*, 3363–3367; e) D. C. G. Götz, T. Bruhn, M. O. Senge, G. Bringmann, *J. Org. Chem.* **2009**, *74*, 8005–8020.
- [17] L. Latos-Grazynski, in *The Porphyrin Handbook* (Eds.: K. M. Kadish, K. M. Smith, R. Guilard), Academic Press, New York, **2000**, vol. 2, pp. 361–416.
- [18] a) L. Giribabu, T. A. Rao, B. G. Maiya, *Inorg. Chem.* **1999**, *38*, 4971–4980; b) L. Giribabu, C. Vijay Kumar, P. Yella Reddy, *Chem. Asian J.* **2007**, *2*, 1574–1580.
- [19] M. W. Schmidt, K. K. Baldrige, J. A. Boatz, S. T. Elbert, M. S. Gordon, J. H. Jensen, S. Koseki, N. Matsunaga, K. A. Nguyen, S. J. Su, T. L. Windus, M. Dupuis, J. A. Montgomery, *J. Comput. Chem.* **1993**, *14*, 1347–1363.
- [20] G. Schaftenaar, J. H. Noordik, *J. Comput.-Aided Mol. Des.* **2000**, *14*, 123–134.

Received: November 25, 2009
 Published Online: February 8, 2010